



Deposited via The University of Sheffield.

White Rose Research Online URL for this paper:

<https://eprints.whiterose.ac.uk/id/eprint/163856/>

Version: Published Version

Article:

Jeng, J., Johnson, S.L., Carlton, A.J. et al. (2020) Age-related changes in the biophysical and morphological characteristics of mouse cochlear outer hair cells. *The Journal of Physiology*, 598 (18). pp. 3891-3910. ISSN: 0022-3751

<https://doi.org/10.1113/jp279795>

Reuse




This article is distributed under the terms of the Creative Commons Attribution (CC BY) licence. This licence allows you to distribute, remix, tweak, and build upon the work, even commercially, as long as you credit the authors for the original work. More information and the full terms of the licence here:

<https://creativecommons.org/licenses/>

Takedown

If you consider content in White Rose Research Online to be in breach of UK law, please notify us by emailing eprints@whiterose.ac.uk including the URL of the record and the reason for the withdrawal request.

Age-related changes in the biophysical and morphological characteristics of mouse cochlear outer hair cells

Jing-Yi Jeng¹, Stuart L. Johnson^{1,2}, Adam J Carlton¹, Lara De Tomasi¹, Richard J. Goodyear³ , Francesca De Faveri¹, David N. Furness⁴, Sara Wells⁵, Steve D. M. Brown⁶, Matthew C. Holley¹, Guy P. Richardson³, Mirna Mustapha^{1,2}, Michael R. Bowl⁶  and Walter Marcotti^{1,2} 

¹Department of Biomedical Science, University of Sheffield, Sheffield, S10 2TN, UK

²Neuroscience Institute, University of Sheffield, Sheffield, S10 2TN, UK

³School of Life Sciences, University of Sussex, Falmer, Brighton BN1 9QG, UK

⁴School of Life Sciences, Keele University, Keele, ST5 5BG, UK

⁵Mary Lyon Centre, MRC Harwell Institute, Oxfordshire, UK

⁶Mammalian Genetics Unit, MRC Harwell Institute, Oxfordshire, UK

Edited by: Kim Barrett & Nathan Schoppa

Key points

- Age-related hearing loss (ARHL) is a very heterogeneous disease, resulting from cellular senescence, genetic predisposition and environmental factors (e.g. noise exposure).
- Currently, we know very little about age-related changes occurring in the auditory sensory cells, including those associated with the outer hair cells (OHCs).
- Using different mouse strains, we show that OHCs undergo several morphological and biophysical changes in the ageing cochlea.
- Ageing OHCs also exhibited the progressive loss of afferent and efferent synapses.
- We also provide evidence that the size of the mechano-electrical transducer current is reduced in ageing OHCs, highlighting its possible contribution in cochlear ageing.

Abstract Outer hair cells (OHCs) are electromotile sensory receptors that provide sound amplification within the mammalian cochlea. Although OHCs appear susceptible to ageing, the progression of the pathophysiological changes in these cells is still poorly understood. By using mouse strains with a different progression of hearing loss (C57BL/6J, C57BL/6NTac, C57BL/6NTac^{Cdh23+}, C3H/HeJ), we have identified morphological, physiological and molecular changes in ageing OHCs (9–12 kHz cochlear region). We show that by 6 months of age, OHCs from all strains underwent a reduction in surface area, which was not a sign of degeneration. Although the ageing OHCs retained a normal basolateral membrane protein profile, they showed a reduction in the size of the K⁺ current and non-linear capacitance, a readout of prestin-dependent electromotility. Despite these changes, OHCs have a normal V_m and retain the

Jing-Yi Jeng received her MSc degree in Biotechnology at National Tsing Hua University (Taiwan) and her PhD in Biomedical Science at The University of Sheffield (UK). Her research aims to understand the physiological mechanisms crucial for the development and ageing of the cochlear hair cells in the mammalian cochlea. She is a Postdoctoral Research Associate within the Hearing Research Group (<https://www.sheffield.ac.uk/hearing>) in the Department of Biomedical Science at The University of Sheffield (UK).



ability to amplify sound, as distortion product otoacoustic emission thresholds were not affected in aged, good-hearing mice (C3H/HeJ, C57BL/6NTac^{Cdh23⁺}). The loss of afferent synapses was present in all strains at 15 months. The number of efferent synapses per OHCs, defined as post-synaptic SK2 puncta, was reduced in aged OHCs of all strains apart from C3H mice. Several of the identified changes occurred in aged OHCs from all mouse strains, thus representing a general trait in the pathophysiological progression of age-related hearing loss, possibly aimed at preserving functionality. We have also shown that the mechano-electrical transduction (MET) current from OHCs of mice harbouring the *Cdh23^{ahl}* allele is reduced with age, highlighting the possibility that changes in the MET apparatus could play a role in cochlear ageing.

(Received 12 March 2020; accepted after revision 25 June 2020; first published online 1 July 2020)

Corresponding author Walter Marcotti: Alfred Denny Building, Western Bank, Sheffield S10 2TN, United Kingdom.
Email: w.marcotti@sheffield.ac.uk

Introduction

Age-related hearing loss (ARHL), also known as presbycusis, is the most common form of age-related sensory disability in humans, affecting ~60% of people by 70 years of age (Bowl & Dawson, 2019). ARHL is a complex disorder with both genetic predisposition and environmental factors (e.g. noise exposure) influencing its progression (Bowl & Dawson, 2019; Liberman, 2017), leading to a decrease in sensitivity threshold and speech discrimination (Gates & Mills, 2005; Gordon-Salant, 2005). Among the most common causes of ARHL are the loss of the sensory inner and outer hair cells (IHCs, OHCs) and their innervation within the cochlea (Liberman, 2017), with OHCs being particularly vulnerable to cochlear ageing (e.g. Kusunoki *et al.* 2004; Sergeyenko *et al.* 2013). Currently, very little is known about the functional changes that occur in ageing OHCs, or if any particular physiological or morphological characteristics are more vulnerable to change during the ageing process.

In mammals, normal hearing depends on the ability of the cochlea to amplify acoustic stimuli (Ashmore, 2019). This amplification is provided by the OHCs, which generate voltage-dependent axial forces driving electromotility (Brownell *et al.* 1985; Ashmore, 1987). Electromotility depends on prestin (encoded by *Slc26a5*: Zheng *et al.* 2000; Liberman *et al.* 2002), a protein expressed in the lateral membrane of mature OHCs (Belyantseva *et al.* 2000; Mahendrasingam *et al.* 2010) that changes conformation according to the membrane potential (Oliver *et al.* 2001). The voltage corresponding to the steepest voltage sensitivity of prestin has been estimated at around -40/-50 mV (Huang & Santos-Sacchi, 1993; Oliver & Fakler, 1999; Bai *et al.* 2019; see also: Ashmore, 2008). This relatively depolarized membrane potential of OHCs *in vivo* is likely to be set by the combined activity of the basolateral hyperpolarizing K⁺ current $I_{K,n}$ (Mammano & Ashmore, 1996; Marcotti & Kros, 1999) and the depolarizing resting mechano-electrical transducer current (Johnson *et al.* 2011). Another key feature of

mature OHCs is that their activity is inhibited by the medial olivocochlear (MOC) efferent system (Liberman, 1980; Simmons *et al.* 1996; Maison *et al.* 2003). The release of acetylcholine (ACh) by the efferent neurons leads to OHC hyperpolarization (Oliver *et al.* 2000), thus reducing the mechanical amplification of the cochlear partition (Guinan, 1996; Fuchs & Lauer, 2019). Although mature IHCs are the primary target of the spiral ganglion afferent neurons (~90–95% type I), OHCs receive the remaining 5–10% (type II: Ryugo, 1992), the role of which seems to be to transmit information about noxious sound stimulations (Fuchs, 2018).

The aim of this study was to identify the initial morphological and physiological changes that occur in ageing OHCs (in the 9–12 kHz cochlear region), using four different mouse strains (C57BL/6J, C57BL/6NTac, C3H/HeJ, C57BL/6NTac^{Cdh23⁺}). We show that by 6 months of age all OHCs from the four mouse strains undergo a reduction in surface area, which was not a sign of apoptosis since even in 14–16-month-old mice OHC loss was minimal and did not affect distortion product otoacoustic emissions (DPOAEs) in the good-hearing mouse strain C3H/HeJ. Although OHC reduction in size was not linked to apoptosis, it seemed to be associated with a loss of basolateral membrane proteins, such as ion channels (KCNQ4) and the motor protein prestin, required for driving non-linear capacitance. Ageing OHCs also exhibited the progressive loss of afferent and efferent synapses. Efferent synapses onto OHCs from C3H/HeJ mice, which show the best hearing profile at the cochlear region used for the *in vitro* experiments (12 kHz), exhibited very little changes with age. Since most of the above changes occurred in OHCs from all mouse strains, we conclude that they represent a general trait in the normal pathophysiological progression in the ageing cochlea. Moreover, these changes could allow OHCs to preserve their functionality in the ageing cochlea. We have also shown that the mechano-electrical transduction (MET) current of OHCs from mice harbouring the *Cdh23^{ahl}* allele is reduced with age. These data highlight

the interesting possibility that alterations in the MET apparatus could contribute to the progression of ARHL as previously suggested (Johnson *et al.* 1997; Noben-Trauth *et al.* 2003).

Materials and methods

Ethics statement

All animal work was performed at the University of Sheffield (UK) and licensed by the Home Office under the Animals (Scientific Procedures) Act 1986. Procedures were approved by the University of Sheffield Ethical Review Committee. Mice had free access to food and water and a 12 h light/dark cycle. Auditory functional measurements were conducted under anaesthesia using ketamine (100 mg kg⁻¹ body weight, Fort Dodge Animal Health) and xylazine (10 mg kg⁻¹, Rompun 2%, Bayer), which were administered with intraperitoneal injection as previously described (Ingham *et al.* 2011). At the end of the procedure, mice were either killed in accordance with schedule 1 of the Act or recovered from anaesthesia with intraperitoneal injection of atipamezole (1 mg kg⁻¹). Mice under recovery from anaesthesia were returned to their cage, placed on a thermal mat, and monitored for 2 to 4 h. Cages were returned to the holding racks once the mice were able to move well and respond to external stimuli. The wild-type C57BL/6NTac, C57BL/6J and C3H/HeJ, and the transgenic C57BL/6NTac^{Cdh23+} mice (Mianné *et al.* 2016) used for the experiments were bred at the MRC Harwell Institute.

Tissue preparation

In vitro recordings were performed from apical-coil OHCs (~9–12 kHz: Muller *et al.* 2005) of acutely dissected organs of Corti from mice of 1–18 months of age. Males and females were killed by cervical dislocation and the inner ear placed in a Petri dish containing ice-cold extracellular solution composed of (in mM): 135 NaCl, 5.8 KCl, 1.3 CaCl₂, 0.9 MgCl₂, 0.7 NaH₂PO₄, 5.6 D-glucose, 10 HEPES-NaOH. Sodium pyruvate (2 mM), amino acids and vitamins were added from concentrates (Thermo Fisher Scientific, UK). The pH was adjusted to 7.5 (osmolality ~308 mmol kg⁻¹). The dissection procedure begins with the removal of the muscles and connective tissue surrounding the inner ear. The 'cleaned' inner ear is then moved to a new Petri dish containing fresh solution (i.e. free from debris). By holding the whole inner ear from the vestibular system with a pair of forceps, the bone covering the part of the apical-coil cochlear turn (around 8–20 kHz: see Ceriani *et al.* 2019) is removed using a second pair of forceps (Dumont #3 or #4, which are further polished using a sharpening stone). This initial

step is aimed at exposing the middle bony-spiral structure containing the cochlear nerve, which is then gently cut with very fine forceps, a procedure that allows the removal of the entire bone covering the apical cochlear coil. When the apical coil is exposed, it is very important to keep the solution clean (i.e. adding fresh ice-cold solution) and avoid touching the delicate organ of Corti, which is where the hair cells are located. This is then followed by the removal of the bone covering the site of the apical coil of the organ of Corti in one single step. The final step requires the use of very fine forceps to cut the auditory nerve and gently remove the apical portion of the organ of Corti, which is then placed in the recording chamber using a small stainless steel spoon (about 4 mm in diameter, custom made). The tip size of the forceps used for this procedure changes depending on the thickness of the bone, which changes with age and between strains; usually we have 3–4 sets of forceps to cover the full range of thicknesses. The same procedure was applied to all dissections performed in this study irrespective of the age of the animal. In the recording chamber, the isolated organ of Corti was immobilized using a nylon mesh fixed to a stainless steel ring and viewed using an upright microscope (Olympus BX51, Japan; Leica, DMLFS, Germany; Nikon, Germany). Hair cells were observed with Nomarski Differential Interface Contrast (DIC) optics (×63 or ×60 water immersion objective) and ×15 eyepieces.

Single-cell electrophysiology

For whole-cell basolateral K⁺ current recordings, experiments were performed as previously described (Corns *et al.* 2018; Ceriani *et al.* 2019). The pipette intracellular solution contained (in mM): 131 KCl, 3 MgCl₂, 1 EGTA-KOH, 5 Na₂ATP, 5 HEPES-KOH, 10 Na-phosphocreatine (pH was adjusted with 1 M KOH to 7.28; osmolality was 294 mmol kg⁻¹). Membrane currents and voltage responses were investigated at room temperature (20–24 °C) using the Optopatch amplifier (Cairn Research Ltd, UK). Data acquisition was controlled by pClamp software using Digidata 1440A boards (Molecular Devices, USA). Recordings were low-pass filtered at 2.5 kHz (8-pole Bessel), sampled at 5 kHz and stored on data-drives for off-line analysis (Origin: OriginLab, USA). Membrane potentials in whole-cell recordings were corrected for the residual series resistance R_s after compensation (usually 70–90%) and the liquid junction potential of -4 mV measured between electrode and bath solutions.

The presence of electromotile activity in OHCs was estimated by measuring nonlinear (voltage-dependent) capacitance using whole-cell patch clamp recordings. In order to block most of the ion channels in hair cells, the pipette intracellular solution contained (in mM): 125 CsCl,

3 MgCl₂, 1 EGTA-CsOH, 5 Na₂ATP, 5 Hepes-CsOH, 5 tetraethylammonium (TEA), 5 4-aminopyridine (4-AP) (pH was adjusted with CsOH to 7.28; osmolality was 280 mmol kg⁻¹). Real-time changes in nonlinear membrane capacitance (C_{N-L}) were investigated using the capacitance track-in-mode of the Optopatch amplifier (Cairn Research Ltd, UK) during the application of a 4 kHz sine wave of 13 mV RMS. From the holding potential of -84 mV, hair cells were subjected to a voltage ramp from -154 mV to +96 mV over 2 s. The capacitance signal from the Optopatch amplifier was filtered at 250 Hz and sampled at 5 kHz.

MET currents in young adult and aged mice were recorded from OHCs of *Tecta*^{EGFP/EGFP}; *Tectb*^{-/-} double knockout mice (*Tecta/Tectb*^{-/-}), in which the tectorial membrane is detached from the OHC hair bundles. MET currents were elicited using a fluid jet from a pipette driven by a 25 mm diameter piezoelectric disc (Corns *et al.* 2014; Corns *et al.* 2018). The fluid jet pipette tip had a diameter of 8–10 μm and was positioned at about 8 μm from the hair bundles to elicit a maximal MET current. Mechanical stimuli were applied as steps or 50 Hz sinusoids. The resting MET current becomes evident when the MET channels shut off in the inhibitory phase of the stimulus: the holding current minus the current present during inhibitory bundle deflection (Corns *et al.* 2014).

Auditory brainstem responses

Auditory brainstem responses (ABRs) were recorded from male and female mice between 1 and 18 months of age. Recordings were performed in a soundproof chamber (MAC-3 Acoustic Chamber, IAC Acoustic, UK) as previously described (Ingham *et al.* 2011). Briefly, stimuli were delivered to the ear by calibrated loudspeakers (MF1-S, Multi Field Speaker, Tucker-Davis Technologies, USA) placed 10 cm from the animal's pinna. Sound pressure was calibrated with a low-noise microphone probe system (ER10B+, Etymotic, USA). Experiments were performed using BioSigRZ software (Ingham *et al.* 2011) driving an RZ6 auditory processor (Tucker-Davis Technologies). Response thresholds were estimated from the resulting ABR waveforms and defined as the lowest sound level where any recognisable feature of the waveform was visible. Each set of ABR data was independently assessed by at least three members of the laboratory without prior knowledge of the mouse strain, age or sex. Responses were measured for click and stimulus pure tones of frequencies between 3 and 42 kHz. Stimulus were typically 0–95 dB sound pressure level (SPL) and presented in steps of 5 dB. The brainstem response signal was averaged over 256 repetitions. Tone bursts were 5 ms in duration with a 1 ms on/off ramp time, and were presented at a rate of 42.6/s.

Distortion product otoacoustic emissions

OHC function was assessed *in vivo* by measuring the distortion product otoacoustic emissions (DPOAEs). Recordings were performed in a soundproof chamber (MAC-3 Acoustic Chamber, IAC Acoustic, UK). DPOAEs were recorded at 2f₁–f₂ in response to primary tones f₁ and f₂, where f₂/f₁ = 1.2. The f₂ level (L2) was set from 20 to 80 dB in 10 dB increments, and the f₁ level (L1) was set equal to L2. Frequency pairs of tones between f₂ = 6.5 kHz and f₂ = 39.2 kHz were presented directly into the ear canal by means of a metal coupler connected to two calibrated loudspeakers (MF1-S, Multi Field Speaker, Tucker-Davis Technologies, USA). The emission signals were recorded by a low-noise microphone (ER10B+: Etymotic Research Inc, USA) connected to the coupler. Experiments were performed using BioSigRZ software driving an RZ6 auditory processor (Tucker-Davis Technologies). The DPOAE thresholds were defined by the minimal sound level where the DPOAEs were above two standard deviation of the noise. The determined DPOAE thresholds were plotted against geometric mean frequency of f₁ and f₂. Stimulus sound pressure levels were typically 0–80 dB SPL, presented in steps of 10 dB. The response signal was averaged over 500 repetitions.

Immunofluorescence microscopy

The dissected inner ears from the mice were fixed with 4% paraformaldehyde in phosphate-buffered saline (PBS, pH 7.4) for 20 min at room temperature. Cochleae were microdissected, rinsed three times for 10 min in PBS, and incubated for 1 h at room temperature in PBS supplemented with 5% normal goat or horse serum and 0.5% Triton X-100. The samples were then incubated overnight at 37°C with the primary antibody in PBS supplemented with 1% of serum. Primary antibodies were: mouse anti-myosin 7a (1:1000, Developmental Studies Hybridoma Bank, #138-1C), rabbit anti-myosin 7a (1:200, Proteus Biosciences, #25-6790), rabbit anti-prestin (1:5000, kindly provided by Robert Fettiplace), rabbit anti-SK2 (1:500, Sigma-Aldrich, P0483) goat anti-choline acetyltransferase (ChAT, 1:500, Millipore, AB144P), and mouse anti-CtBP2 (1:200, Biosciences, #612044). All primary antibodies were labelled with species-appropriate Alexa Fluor or NorthernLights secondary antibody for 1 h at 37°C. Samples were then mounted in VECTASHIELD. The z-stack images were captured with a Nikon A1 confocal microscope equipped with Nikon CFI Plan Apo 60X Oil objective, which is part of the Light Microscope Facility at the University of Sheffield. Image stacks were processed with Fiji Image Analysis software. The number of synaptic ribbons (CtBP2) and SK2 puncta was estimated from the z-stack images of the immunolabelled proteins using Fiji ImageJ. For the SK2 puncta,

the threshold for staining identification was manually set on a per sample basis at a level at which puncta of the expected size, shape and intercellular location were clearly distinct from the background. Within each mouse strain, 1-month and 15-month-old mice were fixed and processed for imaging simultaneously, while 6-month-old mice were done separately. Images were taken within a few days of fixing the samples. To identify the presence of colocalized SK2 and ChAT puncta we used the blob finder function within Arivis Vision4D 3.1 software on Z-projected images. Briefly, images were processed with a Gaussian filter, followed by an automatic seed finding and a watershed algorithm. A threshold at $<1 \mu\text{m}$ was set to define the juxtaposition of SK2 and ChAT puncta and the results were confirmed by visual inspection. Each set of experiments was performed on at least three mice.

RNA isolation, cDNA synthesis, RT-qPCR and gene sequencing

Cochleae were dissected from mice at 1 and 15 months of age and frozen until processing. Total RNA was isolated using the RNeasy-4PCR Total RNA Isolation Kit (Invitrogen, AM1914) and RNA quantity and quality were verified with the Nanodrop. Equal amounts of cDNA were synthesised using the High-Capacity RNA-to-cDNA Kit (Applied Biosystem, 4387406). Following DNase I treatment, quantitative real-time PCRs were performed using QuantStudio 12K Flex Real-Time PCR System and PowerUp SYBR Green Master Mix (Applied Biosystem, A25776). Every sample was run in triplicate in a 386-well plate (StarLab, B2323-3840), with inclusion of appropriate no-RT and no-template controls. The following gene-specific primers were used: *Slc26a5* (5'-CTCTTTGAGTCGTTACCCAG-3' and 5'-GTAATCAGTCCGTAGTCCAAGC-3'); *Ocm* (5'-TGGAGATGGGAAGATTGGG-3' and 5'-GGACTTGGTAAATAGTTCGGG-3'); *Cdh23* (5'-GCACCCACATTCACAAC-3' and 5'-AGTCTAGCTCCTGAATCACG-3'), *Pcdh15* (5'-GTTTCTGCCTTGTGTCTTGTG-3' and 5'TGTTTCGGTCCTGATCAATGG-3'). Expression levels were normalized using the housekeeping gene *Hprt* (5'-GCTTGCTGGTGAAAAGGAC-3' and 5'-AGATTCAA CTTGCGCTCATC-3') and analysed using the $2^{-\Delta\Delta C_T}$ method.

In order to investigate whether *Tecta/Tectb* double knockout mice (*Tecta/Tectb*^{-/-}) harbour the *Cdh23*^{ahl} allele (Johnson *et al.* 1997; Noben-Trauth *et al.* 2003), we performed DNA sequencing. Genomic DNA from the animals was extracted using NaOH. The targeted region was PCR amplified using GoTaq Master Mixes (M7123, Promega) and primers 5'-TCAGGCTCCCCTGC TTCTAT-3' and 5'-CCAAGCTGTTCCCTGGTAGCT-3'. PCR products were purified and sequenced by Sanger

sequencing using the DNA sequencing service from Core Genomic Facility, University of Sheffield.

Scanning electron microscopy (SEM)

For SEM, cochleae were excised from aged C57BL/6N mice (15 months). They were fixed by intralabyrinthine perfusion using a fine hypodermic needle through the round window with 2.5% vol/vol glutaraldehyde in 0.1 M sodium cacodylate buffer containing 2 mM calcium chloride (pH 7.4) and then immersed in this fixative for 2 h. They were stored in fixative diluted 1/10th in buffer and subsequently dissected by removing the bone from the apical coil to expose the organ of Corti and then immersed in 1% osmium tetroxide in the cacodylate buffer for 1 h. For osmium impregnation, which avoids gold coating, cochleae were incubated in solutions of saturated aqueous thiocarbonylhydrazide (20 min) alternating with 1% osmium tetroxide in buffer (2 h) twice (the OTOTO technique) (Furness & Hackney, 1986). They were dehydrated through an ethanol series and critical point dried using CO₂ as the transitional fluid, then mounted on specimen stubs using conductive silver paint (Agar Scientific, Stansted, UK) and examined in a Hitachi S4500 field emission SEM operated at 5 kV accelerating voltage.

Toluidine blue staining

After glutaraldehyde fixation, cochleae were washed three times in 0.1 M sodium cacodylate buffer pH 7.2 and post-fixed in 1% osmium tetroxide in 0.1 M sodium cacodylate buffer for 3 h at room temperature. Samples were then washed three times in sodium cacodylate buffer and decalcified in 0.5 M EDTA pH 8.0 containing 0.1% glutaraldehyde for 3 days at 4°C. Samples were then washed briefly in water, dehydrated through an ascending ethanol series, equilibrated in propylene oxide and embedded in epoxy (TAAB 812) resin. Blocks were cured at 60°C for 24 h and trimmed with a glass knife after which semi-thin 1 micron thick sections were cut on a Reichert Ultracut E ultramicrotome using a histo-grade Diatome diamond knife. Sections were dried onto glass slides and stained briefly with toluidine blue before viewing on a Zeiss Axioplan 2 wide-field microscope. Images were captured with a Spot RT digital camera.

Statistical analysis

Statistical comparisons of means were made by Student's two-tailed *t* test or for multiple comparisons, analysis of variance (one-way and two-way ANOVA followed by Tukey's or Sidak's post hoc test). $P < 0.05$ was selected as the criterion for statistical significance. Only mean

values with a similar variance between groups were compared. Mean values are quoted in text and figures as means \pm SD. For DPOAE experiments, due to the presence of ‘not found’ values (i.e. above the upper threshold limit of our equipment), the non-parametric aligned ranks transformation two-way ANOVA was used. Mann–Whitney U-test was used for pairwise comparisons with Bonferroni-adjusted P values) statistical test. Data are quoted as median, and first and third quartiles.

Results

Mouse mutants have been instrumental in the identification and characterization of genes underlying congenital and early-onset hearing loss (Mianné *et al.* 2016; Bowl *et al.* 2017). In addition, the mouse has been utilized for the study of ARHL, taking advantage of the fact that different inbred strains, while having very similar hearing thresholds when young, exhibit differing rates of hearing loss with age (Ohlemiller *et al.* 2016). Some strains, such as C3H/HeJ and CBA, are labelled ‘good’ hearing strains and show a very slow decline in their hearing thresholds with age (Trune *et al.* 1996; Spongr *et al.* 1997; Sha *et al.* 2008). However, other strains, such as C57BL/6NTac and C57BL/6J, exhibit an early progressive hearing loss (starting from 3 months of age at high frequency), which is due to the presence of a fixed hypomorphic allele in *Cadherin 23* (*Cdh23^{ahl}*; Johnson *et al.* 1997; Noben-Trauth *et al.* 2003). *Cdh23* encodes cadherin-23 that, together with protocadherin-15, forms the stereocilia tip links required for gating the mechano-electrical transducer channels (Kazmierczak *et al.*, 2007; Richardson *et al.* 2011). A recent study has shown that when the *Cdh23^{ahl}* allele in C57BL/6NTac mice

is ‘corrected’, using CRISPR/Cas9 homology-directed repair (C57BL/6NTac^{*Cdh23*+}), the mice exhibit improved age-related hearing with normal thresholds observed at 8 months of age (Mianné *et al.* 2016). Because of the complexity and heterogeneous nature of ARHL, we investigated the function of OHCs in mouse strains that show early-onset hearing loss (C57BL/6NTac: 6N; C57BL/6J: 6J) and strains that have good age-related hearing (C57BL/6NTac^{*Cdh23*+}: 6N-Repaired; C3H/HeJ: C3H), with the aim of identifying early signs of any morphological and physiological change in OHCs associated with ARHL.

Age-related changes in hearing function

We initially determined the hearing loss in the four mouse strains, which were kept under the same environmental conditions, in order to provide a more comprehensive understanding of the progression of the pathology. ABRs, which indicate the activity of the afferent auditory pathway downstream of IHCs, were made using the same experimental set-up. At 12–14 months of age, good-hearing C3H mice had ABR thresholds for click and pure-tone evoked ABRs (Fig. 1A,B) comparable to those published previously (Trune *et al.* 1996). ABR thresholds to clicks were significantly different among strains ($P < 0.0001$, one-way ANOVA). Compared with C3H mice, aged-matched 6J and 6N strains showed significantly increased ABR thresholds for clicks (6J, $P < 0.001$; 6N, $P < 0.05$; Tukey’s post hoc test, one-way ANOVA: Fig. 1A). 6N-Repaired mice had ABR click stimulus thresholds comparable to C3H mice ($P > 0.05$), but significantly lower values than those measured in the co-isogenic 6N strain ($P < 0.01$) and 6J mice ($P < 0.001$:

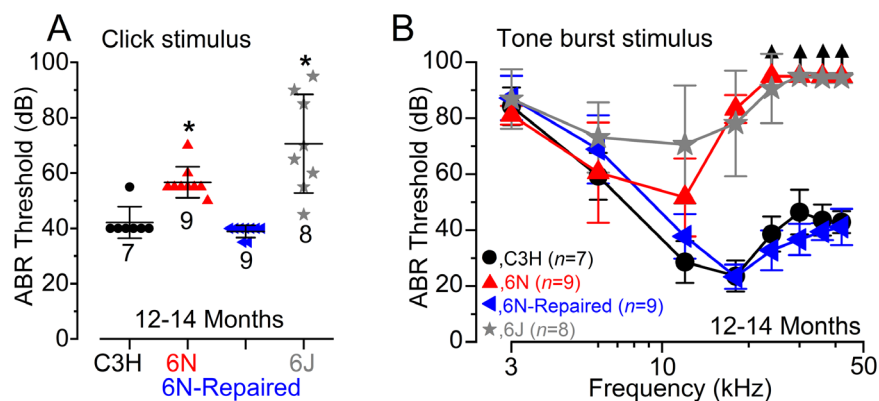


Figure 1. ABR thresholds evoked by frequency-specific stimuli

A and B, mean ABR thresholds for clicks (A) and frequency-specific pure-tone stimulation from 3 kHz to 42 kHz (B) obtained from C3H, 6N, 6N-Repaired and 6J mice at 12–14 months of age. The arrows in B represent values above the upper threshold limit of our equipment (95 dB SPL). ABR thresholds were significantly elevated in 6J and 6N mice compared with both C3H and 6N-Repaired mice. For clicks: one-way ANOVA from single data points was: $P < 0.0001$. For frequency-specific stimulations, two-way ANOVA was $P < 0.0001$. For post hoc test comparisons, see Results. *indicates statistical significance when compared to C3H mice. Number of animals tested (males and females) is indicated by ‘n’ and shown next to the different mouse strains. Values are means \pm SD.

Tukey's post hoc test, one-way ANOVA) (Fig. 1A). ABR thresholds for pure tones were not significantly different between C3H and 6N-Repaired ($P = 0.140$), or between 6N and 6J ($P = 0.979$, Tukey's post hoc test, two-way ANOVA). However, they were increased in the early-onset hearing loss (6N and 6J) compared with C3H and 6N-Repaired ($P < 0.0001$, Tukey's post hoc test for all four strain combinations, two-way ANOVA) (Fig. 1B). All four mouse strains showed similar ABR thresholds only at 3 kHz ($P = 0.3168$) and 6 kHz ($P = 0.1376$; Tukey's post hoc test, one-way ANOVA).

In order to investigate the specific contribution of OHCs to these hearing phenotypes, we performed DPOAEs (Figs 2 and 3), which are readouts of cochlear amplification caused by the displacement of OHC stereociliary bundles during sound-induced motion of the cochlear partition. We initially compared the DPOAE thresholds between males and females at 13–14 months of age, and we found no significant differences in all four strains (C3H,

$P = 0.3853$; 6N, $P = 0.5136$; 6N-Repaired, $P = 0.1988$; 6J, $P = 0.1956$, aligned ranks transformation two-way ANOVA). Because no statistical significance was detected between strain-matched males and females, data from males and females were pooled together to investigate possible inter-strain differences in DPOAE thresholds (Fig. 2). We found no significant difference between C3H and 6N-Repaired mice ($P = 0.5737$) or between 6N and 6J mice ($P = 0.1800$, aligned ranks transformation two-way ANOVA). However, DPOAE thresholds were significantly raised in both 6N and 6J mice compared with those recorded from C3H and 6N-Repaired mice ($P < 0.0001$ for all four combinations, aligned ranks transformation two-way ANOVA). These results also indicate that OHC defects are partially responsible for the different ABR thresholds between early-onset hearing loss and good-hearing mice (Fig. 1). We then used male mice to investigate age-related changes in DPOAE thresholds (6–24 kHz range: Fig. 3A–F). As expected,

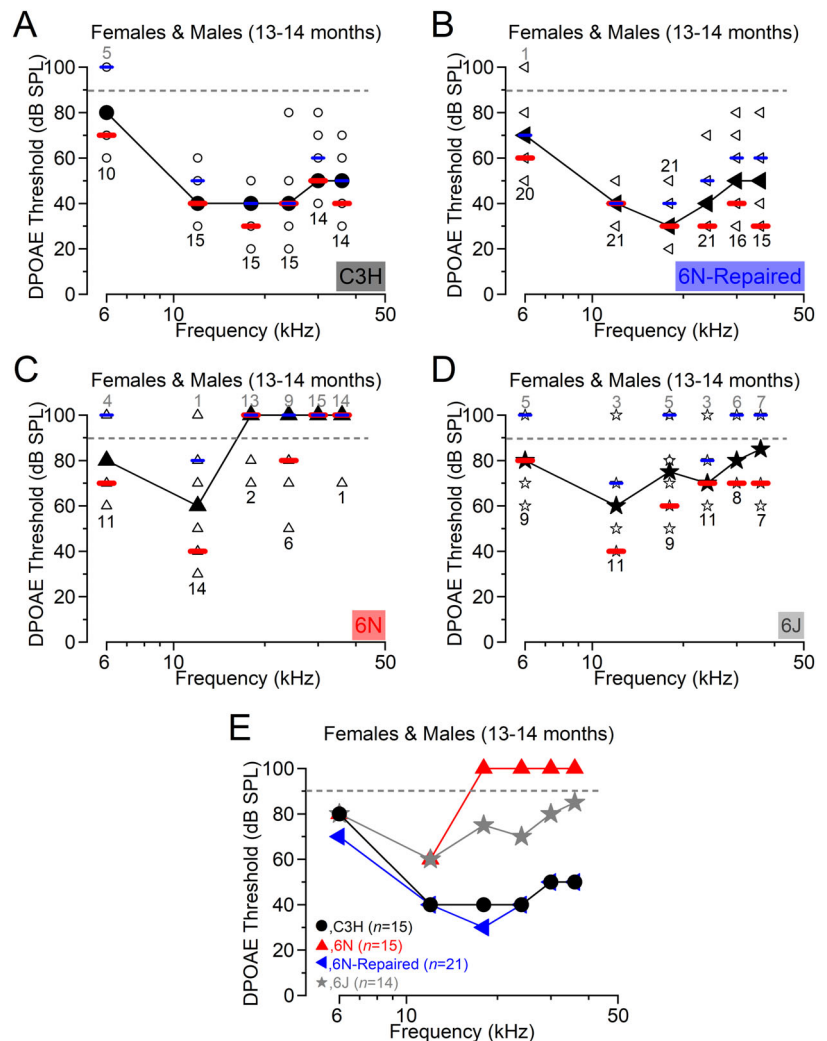


Figure 2. DPOAE thresholds in aged male and female mice

A–E, DPOAE thresholds measured in both males and females from 13–14 months old C3H (A, 15 mice), 6N-Repaired (B, 21 mice), 6N (C, 15 mice) and 6J (D, 14 mice) mice. Panel E shows the direct comparison of age-related changes in the median DPOAE threshold values for the four mouse strains. Because of the presence of ‘not found’ values (i.e. above the upper threshold limit of our system, 80 dB) in all mouse strains investigated (see Methods), in this and the following figures, DPOAE threshold values are shown as median (black line and circles), first (red lines) and third (blue lines) quartiles. Single values are reported as open circles. The number of mice with ‘found’ and ‘not found’ values at each frequency is shown below (black) and above (grey) the median, respectively.

the C3H and 6N-Repaired mice showed no significant change in DPOAE thresholds between 1 and 17 months of age (C3H, $P = 0.4791$, Fig. 3A, D; 6N-Repaired, $P = 0.8290$, Fig. 3B, E), while early-onset hearing loss mice exhibited highly increased DPOAE thresholds (6N, $P < 0.0001$, Fig. 3C, F, aligned ranks transformation two-way ANOVA). At the 12 kHz region, which was used for the *in vitro* measurements described below, we found that DPOAE values were significantly different between strains ($P < 0.0001$, aligned ranks transformation two-way ANOVA). At 14–17 months, DPOAE thresholds were highly elevated in 6N compared with both C3H and 6N-Repaired strains ($P = 0.0108$; $P = 0.0002$, respectively), but not significantly different between C3H

and 6N-Repaired mice ($P = 0.5808$, Tukey's post hoc test from aligned ranks transformation two-way ANOVA; see Methods). These findings are in agreement with the extensive literature describing the progressive changes in DPOAE threshold in early-onset hearing loss and good-hearing mice (e.g. Spongr *et al.* 1997; Jimenez *et al.* 1999; Zheng *et al.* 1999).

The biophysical properties of OHCs in ageing mice

In order to investigate possible changes in the biophysical properties of OHCs in ageing mice, we performed electrophysiological recordings from apical (~9–12 kHz) OHCs

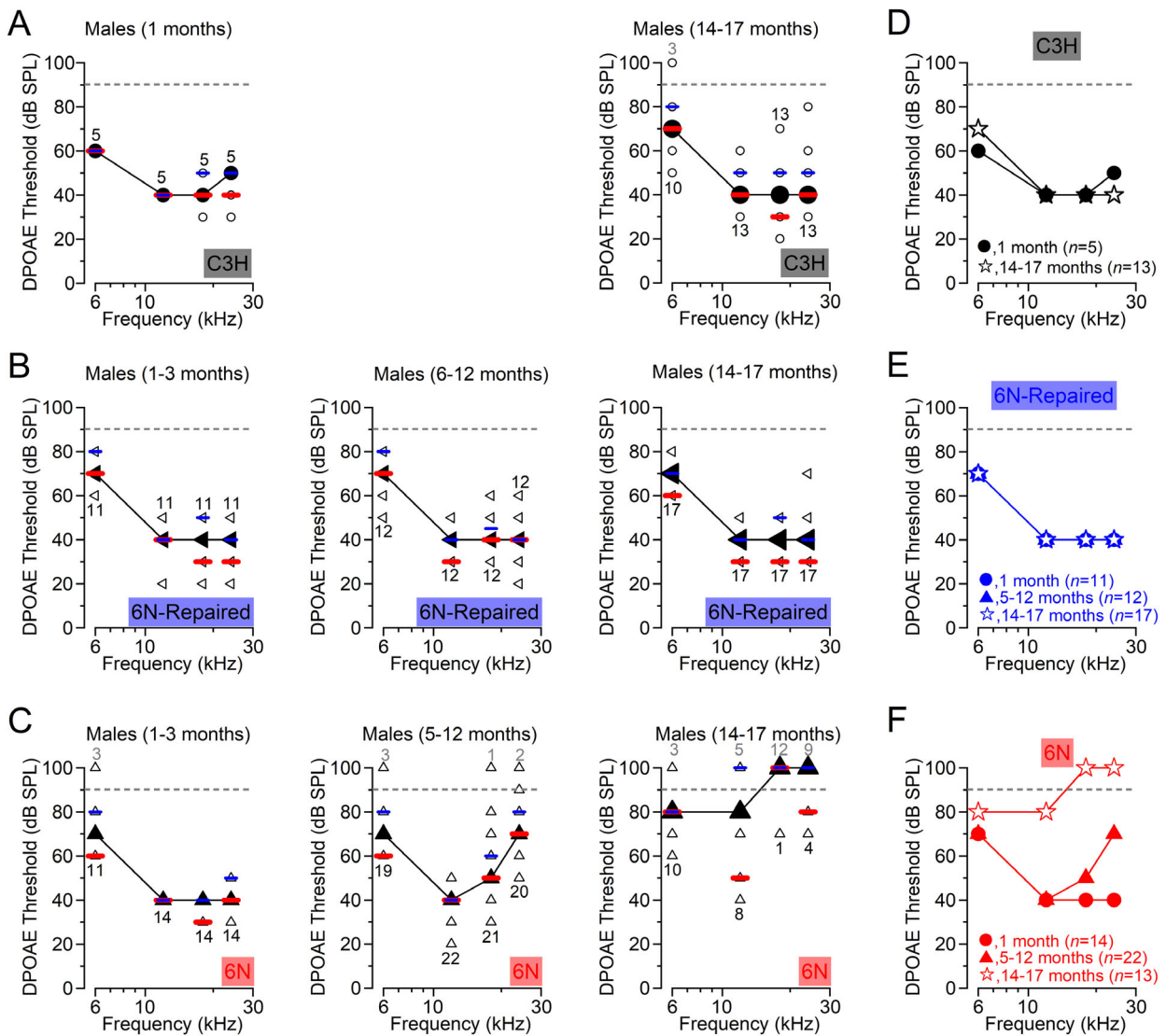


Figure 3. Age-related changes in DPOAE thresholds in male mice

A–D, DPOAE thresholds from males of C3H (A), 6N-Repaired (B) and 6N (C) at different ages for frequencies between 6 and 24 kHz. The number of mice with ‘found’ and ‘not found’ values at each frequency is shown below and above the median, respectively. D–F, comparison of age-related changes in the median DPOAE threshold values (from panels A–C) for the different mouse strains. Number of mice used for each strain/age is also shown.

of 12–13-month-old male and female mice. Mature mouse OHCs express a negatively activating K^+ current called $I_{K,n}$, which is carried by KCNQ4 channels (*Kcnq4* gene; Kubisch *et al.* 1999) and represents the major K^+ current present in these cells (Marcotti & Kros, 1999). Using whole-cell patch clamp, we recorded the K^+ currents from OHCs by applying a series of depolarizing voltage steps in 10 mV increments from -124 mV (holding potential was -84 mV). We found that a large $I_{K,n}$ was

present in the OHCs of females and males from all four mouse strains (Fig. 4A–D shows female OHCs). The peak current–voltage (I – V) relationship of the total K^+ current (I_K ; Fig. 4E) in OHCs was not significantly different in females and males of all four mouse strains (C3H: $P = 0.6558$; 6N-Repaired: $P = 0.3563$; 6N: $P = 0.7571$; 6J: $P = 0.2578$, two-way ANOVA). The size of the total K^+ current (Fig. 4F), which was measured at 0 mV for consistency with previously published work in adult

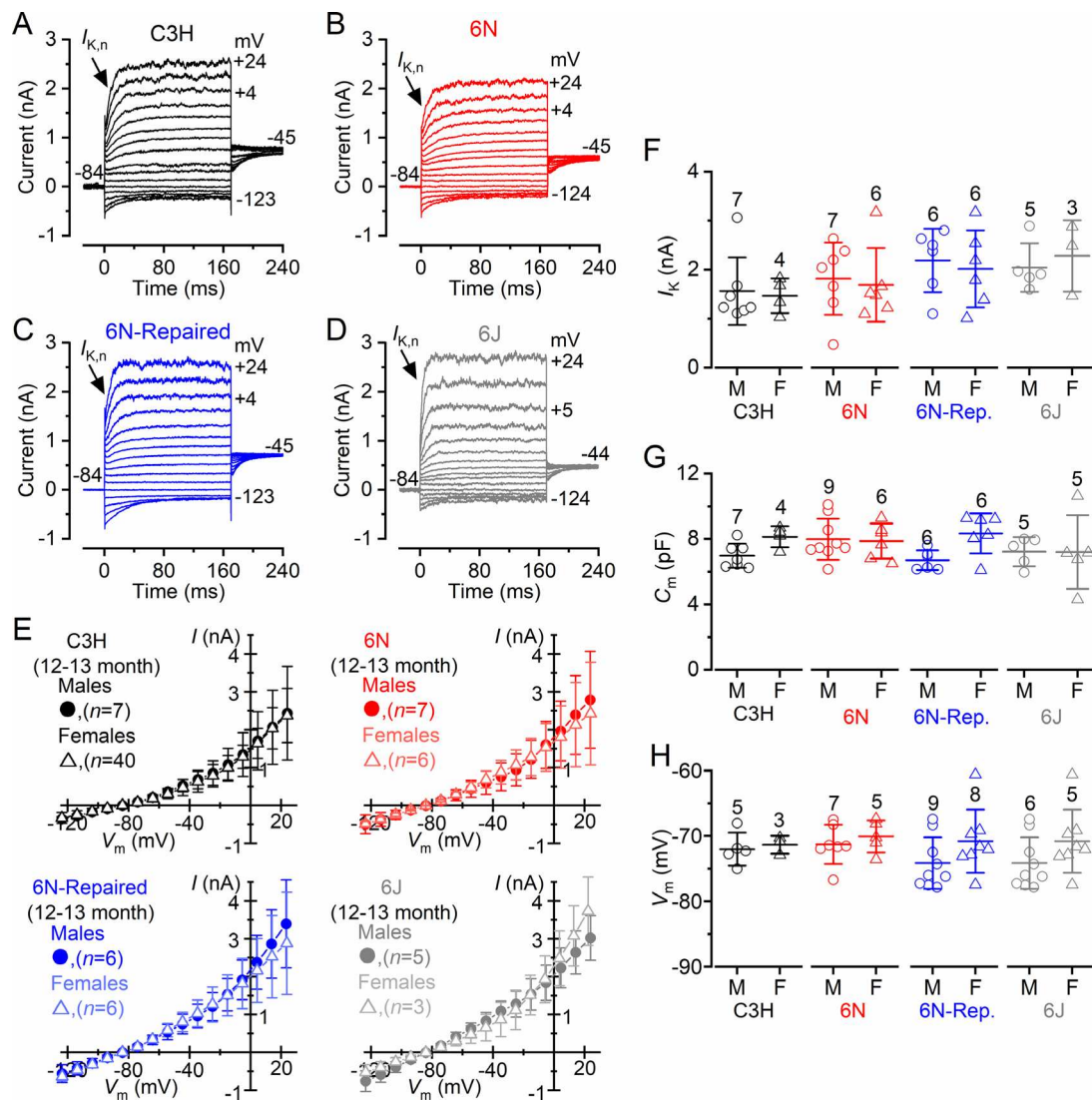


Figure 4. Biophysical properties of outer hair cells in one-year-old males and females

A–D, potassium currents recorded from apical coil outer hair cells (OHCs) of 12–13-month-old females of C3H (A), 6N (B), 6N-Repaired (C) and 6J (D) using 10 mV depolarizing voltage steps from -124 mV to the various test potentials shown by some of the traces. The activation of the adult-type current $I_{K,n}$ (indicated by the arrows) was present in all OHCs. E, average current–voltage (I – V) curves obtained from 12–13-month-old OHCs from females and males of the above four mouse strains. F, average size of the peak K^+ current measured at the membrane potential of 0 mV, as previously described (Marcotti & Kros, 1999), in OHCs from males and females of the different mouse strains. G and H, average OHC membrane capacitance (C_m : G) and resting membrane potential (V_m : H) in the different mouse strains. In panels F–H, individual cell values are also plotted as open symbols. Note that 6N-Repaired was abbreviated as 6N-Rep. Number of OHCs investigated is shown above the data points. Number of mice used: 12 C3H, 15 6N, 12 6N-Repaired and 9 6J. Values are means \pm SD.

OHCs (Marcotti & Kros, 1999), was similar across all four mouse strains and sex ($P = 0.9218$, two-way ANOVA). We then investigated two crucial biophysical properties of OHCs, their membrane capacitance (C_m), which provides an indication of the cell surface area, and their resting membrane potential (V_m). Both were comparable between strains and sex (C_m : $P = 0.1990$, Fig. 4G; V_m : $P = 0.4705$, Fig. 4H, two-way ANOVA). The resting V_m of OHCs was measured under whole-cell current clamp conditions and using 1.3 mM extracellular Ca^{2+} , which also includes the effect of the very small resting MET current. MET channel blockers were not used because they normally affect the

basolateral membrane conductances (e.g. Kenyon *et al.* 2017).

Following this initial characterization, we sought to investigate whether the biophysical characteristics of OHCs changed with age. Considering that we did not find any specific sex differences in aged mice in terms of hearing ability (Fig. 2) or OHC biophysics (Fig. 4), the following experiments are reported by combining the data from males and females. The size of I_K decreased significantly with age in each mouse strain (C3H: $P = 0.0096$; 6N-Repaired: $P = 0.0018$; 6N: $P = 0.0292$; 6J: $P = 0.0007$, one-way ANOVA: Fig. 5A–C), but was not significantly

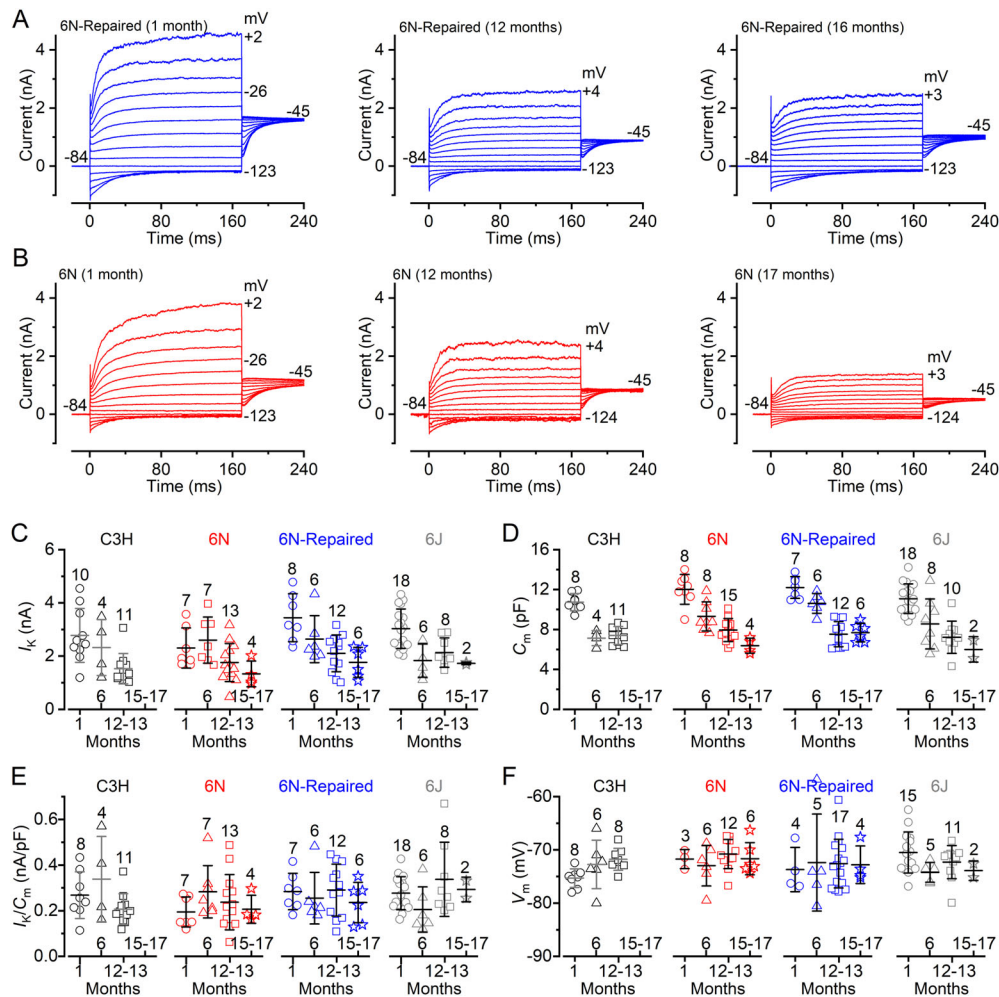


Figure 5. Age-related changes in outer hair cell biophysical characteristics in males and females

A and B, example of K^+ currents recorded from apical coil outer hair cells (OHCs) of male 6N-Repaired (A) and 6N (B) mice at 1 month (left panels), 12 months (middle panels) and 16–17 months (right panels) of age. Currents were recorded using the voltage protocol described in Fig. 4. C, peak K^+ current (I_K) measured at the step potential of 0 mV from all four mouse strains at different ages. D, membrane capacitance (C_m) of OHCs as a function of age in the four mouse strains. E, normalized peak I_K (panel C) to the corresponding C_m (panel D) for each OHC tested. F, resting membrane potential (V_m) as a function of age in all the above mouse strains. In panels C–F, single cell values are also shown behind the average data. Number of OHCs investigated is shown above the average data points. Number of mice used: C3H (1 month: 6; 6 months: 6; 12–13 months: 12), 6N (1 month: 5; 6 months: 8; 12–13 months: 15; 15–17 months: 4), 6N-Repaired (1 month: 7; 6 months: 5; 12–13 months: 12; 15–17 months: 4) and 6J (1 month: 19; 6 months: 7; 12–13 months: 9; 15–17 months: 2). For statistical analysis, see Results. Values are means \pm SD.

different between strains ($P = 0.1267$, all strains in the 1–13 month range; $P = 0.1484$, three strains in the 1–17 month range, two-way ANOVA). Within each strain and over the full age range investigated, the C_m of OHCs was also significantly reduced with age ($P < 0.0001$ in each of the four strains, one-way ANOVA: Fig. 5D), with OHC surface being reduced by $\sim 40\%$ in 6J, 6N and 6N-Repaired and $\sim 25\%$ in C3H mice by 15–17 months. This reduction was not significantly different between strains ($P = 0.1243$, all strains in the 1–13 month range; $P = 0.4959$, three strains in the 1–17 month range, two-way ANOVA). We have also found that C_m at 6 months was already significantly smaller than that at 1 month in 6J, 6N and C3H mice ($P < 0.0001$), but not in 6N-Repaired mice ($P = 0.0727$, Tukey's post hoc test, one-way ANOVA). When the size of I_K in OHCs was normalized to their respective C_m (i.e. current density), it was no longer significantly different for any of the four mouse strains (C3H: $P = 0.1125$; 6N-Repaired: $P = 0.7086$; 6N: $P = 0.4292$; 6J: $P = 0.1577$, one-way ANOVA, Fig. 5E), and also between strains (four strains in the 1–13 month age range: $P = 0.0537$; three strains in the 1–17 month range $P = 0.3055$, two-way ANOVA). Despite the reduced size of I_K , the V_m of OHCs remained stable until at least 16–17 months of age in all mouse strains investigated (C3H: $P = 0.0622$; 6N-Repaired: $P = 0.9826$; 6N: $P = 0.5555$; 6J: $P = 0.1125$, one-way ANOVA, Fig. 5F), and also between strains (four strains in the 1–13 month age range: $P = 0.2861$; three strains in the 1–17 month range $P = 0.7763$, two-way ANOVA).

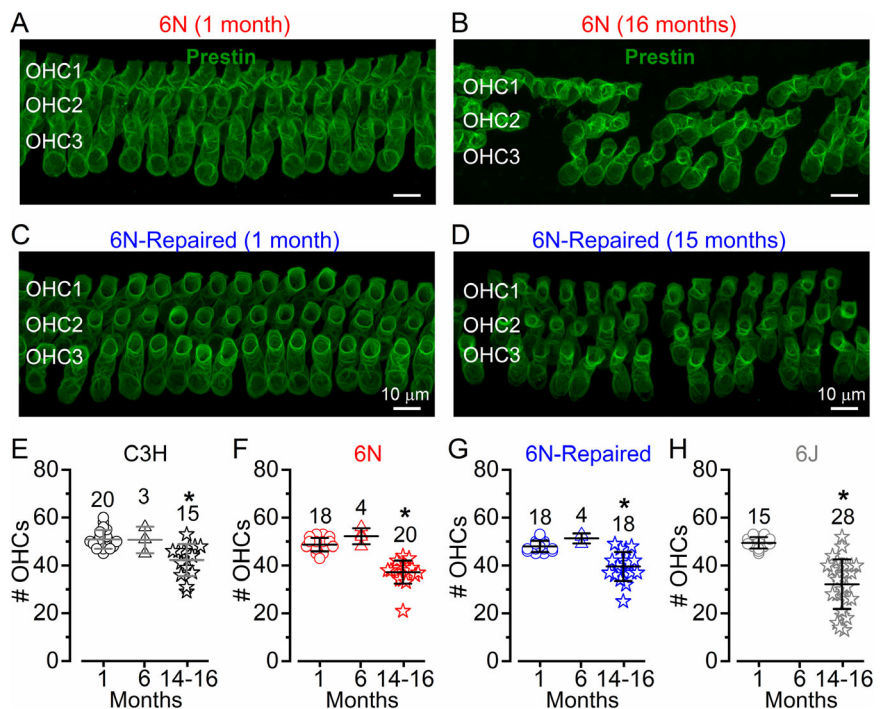
Electromotility is maintained with ageing

One of the characteristic signatures of mature OHCs is the expression of the motor protein prestin (gene name: *Slc26a5*), which drives their somatic motility and thus generates DPOAEs. Therefore, we investigated whether prestin was maintained in ageing OHCs. We found that prestin was expressed in ageing OHCs from all four mouse strains until at least 16 months of age (6N and 6N-repaired: Fig. 6A–D). Since prestin is also used as an OHC marker, it allowed us to investigate any change in the number of OHCs present in the equivalent apical coil region used to perform the above electrophysiological experiments. Myosin 7a antibodies (e.g. Fig. 8) were also used as an additional hair cell marker to avoid underestimating the loss of OHC number with age due to the reduced expression of prestin. We found that the number of OHCs, which was measured over a distance of 140 μm in the ~ 9 –12 kHz region, remained unchanged between 1 and 6 months of age in C3H ($P = 0.9999$), 6N ($P = 0.2510$) and 6N-Repaired mice ($P = 0.9981$, Tukey's post hoc test, one-way ANOVA). However, by 14–16 months of age the number of OHCs significantly decreased compared with one month in all four strains (C3H: $P = 0.0019$, 6N-Repaired: $P = 0.0018$, 6N: $P < 0.0001$, 6J: $P < 0.0001$, one-way ANOVA; Fig. 6E–H).

Although aged OHCs expressed the motor protein prestin (Fig. 6), we sought to test whether it was able to induce voltage-dependent changes in OHC motility (Zheng *et al.* 2000; Liberman *et al.* 2002). OHC electromotile activity can be assessed by either measuring OHC movement

Figure 6. Prestin expression and age-related changes in the number of outer hair cells

A–D, maximum intensity projections of confocal z-stacks taken from the apical cochlear region of 1 month and aged 6N (A and B) and 6N-Repaired (C and D) mice. Outer hair cells (OHCs) were stained with antibodies against prestin (green). Scale bars: 10 μm . E–H, number of OHCs present in a 140 μm region from the apical coil of 1, 6 and 14–16-month-old mice from the four mouse strains used in the previous electrophysiological experiments. OHC counting from individual cochleae (open symbols) are plotted behind the average data and were collected from both males and females. Number of mice investigated is shown above the data points. Values are means \pm SD. For statistical analysis, see Results.



visually, or by using the non-linear (voltage-dependent) capacitance change (C_{N-L}) under whole-cell patch clamp, which is an electrical signature of electromotility (e.g. Abe *et al.* 2007; Bai *et al.* 2019; Zhai *et al.* 2020; Jeng *et al.* 2020). In the present study we preferred to use C_{N-L} because it is particularly difficult to measure visual OHC motility on a precise horizontal plane and because displacement can be misleading through its dependence on intracellular turgor pressure, which is variable. We found that the maximum size of C_{N-L} recorded in OHCs decreased significantly between 1 month and aged 6N ($P = 0.0013$), 6J ($P = 0.0160$) and 6N-Repaired mice ($P = 0.0017$, Tukey's post hoc test, one-way ANOVA), but was similar among strains ($P = 0.6120$, two-way ANOVA) (Fig. 7A–C). When the C_{N-L} was normalized to the OHC membrane capacitance, there was no significant difference among all data groups ($P = 0.0589$, one-way ANOVA) or between strains ($P = 0.2306$, two-way ANOVA) (Fig. 7D). These

data indicate that the electromotile activity is maintained in aged OHCs, but reduced in amplitude most likely due to the cells becoming smaller and losing some prestin in their lateral membrane (Fig. 7D). We have also investigated whether the expression level of prestin was affected in the aged cochlea by performing quantitative PCR experiments at 1 and 15–17-month-old 6N and 6N-Repaired mice. We found that the expression of prestin (*Slc26a5*) was significantly reduced in both aged mouse strains (6N, $P = 0.0117$; 6N-Repaired, $P = 0.0248$, Student's *t* test) (Fig. 7E). We also found that *Ocm*, which encodes for the main Ca^{2+} binding protein oncomodulin expressed in OHCs (Simmons *et al.* 2010), was significantly reduced with age (6N, $P = 0.0110$; 6N-Repaired, $P = 0.0028$, Student's *t* test; Fig. 7F) in both strains. Although these qPCR experiments are intrinsically biased by the fact that OHC loss along the length of the cochlea is likely to be different among mouse strains (e.g. Hequembourg

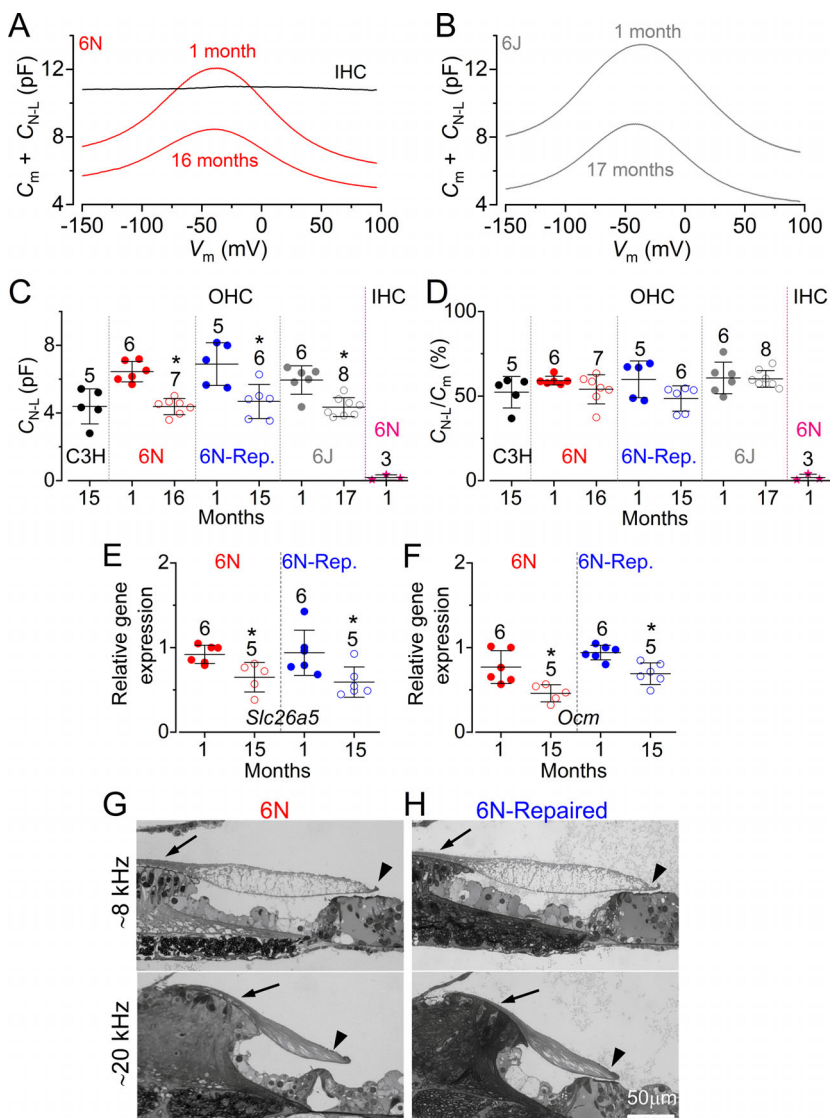


Figure 7. Aged outer hair cells exhibit electromotility

A and B, examples of voltage-dependent non-linear capacitance (C_{N-L}) recorded in apical-coil outer hair cells (OHCs) from 1-month and aged 6N (A) and 6J (B) mice by applying a voltage ramp from -154 mV to $+96$ mV over 2 s. Note that the cell membrane capacitance (C_m) was added to the measured C_{N-L} . C_{N-L} was absent in the non-electromotile inner hair cells, which was used as a control for our experiments. C and D, average C_{N-L} was reduced in OHCs from both mouse strains with age (C), but not after normalization to the OHC membrane capacitance C_m (D). C_{N-L} was calculated as the difference between the peak of the recording near -40 mV and the lowest value at positive membrane potentials. For statistical analysis, see Results. Number of cells investigated is shown above the data. Individual measurements are plotted behind the average data points and were collected from both males and females. Values are means \pm SD. E, F, quantitative real-time PCR (qPCR) from 6N and 6N-Repaired mice at 1 and 15 months of age. Genes investigated: *Slc26a5* (E, prestin) and *Ocm* (F, oncomodulin). Number of mice tested is shown above the data. Values are means \pm SD. G and H, toluidine blue stained semi-thin plastic sections from the 8 kHz and 20 kHz region of the cochlea of 17-month-old 6N (G) and 6N-Repaired mice (H) mice. The tectorial membrane (TM) is attached to the spiral limbus (arrows) and lying on top of the OHCs (arrowheads).

& Liberman, 2001; Francis *et al.* 2003; Zachary & Fuchs, 2015; Sha *et al.* 2008; Ohlemiller *et al.* 2010), the results show a similar reduction in prestin level between the early-onset (6N) and late-onset (6N-Repaired) hearing loss mice, suggesting that its expression level is likely to be similarly affected by ageing.

OHC function also depends upon the tectorial membrane (TM), which is an acellular structure attached to the stereociliary bundles of the OHCs that gradually degrades with age especially in C57BL/6J mice (Goodyear *et al.* 2019). The presence and structure of the TM was investigated using light microscopy and toluidine blue staining. In both 6N and 6N-Repaired mice, the TM was attached medially to the spiral limbus, and laterally sitting atop the OHC stereociliary bundles (Fig. 7G, H), indicating a similar gross structural organization in 17-month-old mice. However, a recent ultrastructure study has shown that the TM progressively detaches from the spiral limbus in very old CBA mice (Bullen *et al.* 2019), indicating some possible strain differences.

Afferent and efferent synapses are reduced in aged OHCs

We evaluated the number of afferent synapses on OHCs from 6N, 6J, 6N-Repaired and C3H mice using an anti-CtBP2 antibody to label the presynaptic ribbon protein RIBEYE. We found that CtBP2 puncta were present at the OHC presynaptic site in the different mouse strains (Fig. 8A, B for 6N and 6N-Repaired mice). The number of CtBP2 puncta in OHCs, over a distance of 140 μm in the ~9–12 kHz region, was significantly different when comparing strains tested at 1, 6 and 15 months (C3H, 6N and 6N-Repaired: $P = 0.0025$) or all four strains tested at 1 and 15 months ($P = 0.0054$, two-way ANOVA). Within each strain, the number of CtBP2 puncta decreased significantly in all strains (C3H and 6N-Repaired: $P < 0.0001$, 6N: $P = 0.0090$, one-way ANOVA; 6J: $P < 0.0001$, Student's *t* test, Fig. 8C–F).

Mature OHCs are mainly innervated by the cholinergic MOC neurons (Liberman, 1980; Maison *et al.* 2003), which release the neurotransmitter acetylcholine (ACh) (Simmons *et al.* 1996). The role of the MOC system is to modulate OHC electromotility and thus mechanical amplification in the cochlear partition (Guinan, 1996). The effects of efferent activity on OHCs is inhibitory because the release of ACh causes Ca^{2+} influx through $\alpha 9\alpha 10$ -nAChRs, which leads to the activation of a hyperpolarizing current through small-conductance Ca^{2+} -activated K^+ channels (SK2: Oliver *et al.* 2000; Katz *et al.* 2004; Lioudyno *et al.* 2004; Marcotti *et al.* 2004). We investigated whether the efferent innervation was retained in the aged cochlea of all four mouse strains by immunolabelling with a choline acetyl transferase (ChAT) antibody, which labels the presynaptic efferent terminals, and with the postsynaptic SK2 antibody. We found that juxtaposed SK2 channels (in OHCs) and ChAT-immunoreactivity (efferent terminals) were still present in most of the remaining OHCs of 15-month-old mice (Fig. 9A, B for 6N and 6N-Repaired mice). The number of SK2 puncta per OHC, within a cochlear

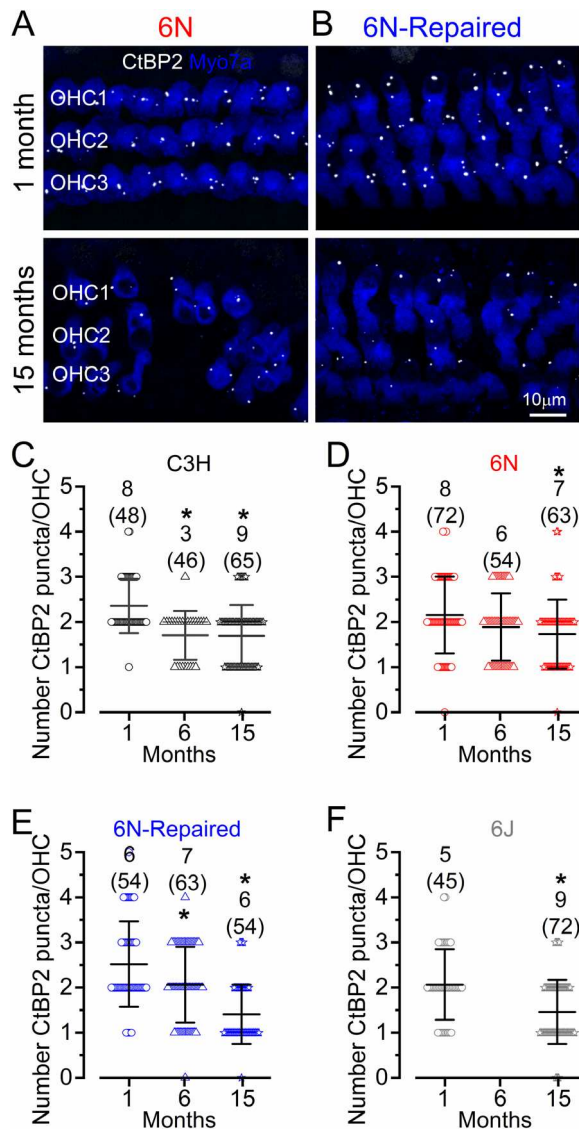


Figure 8. Ribbon synapse number is reduced in outer hair cells from aged mice

A and B, maximum intensity projections of confocal z-stacks taken from the apical cochlear region of 6N (A) and 6N-Repaired (B) mice at 1, 6 and 15 months using antibodies against CtBP2 (ribbon synaptic marker: white). Myosin 7a (Myo7a) was used as a hair cell marker (blue). Scale bar 10 μm. C–F, number of CtBP2 puncta as a function of age in OHCs from C3H (C), 6N (D), 6N-Repaired (E) and 6J (F) mice. Data are plotted as mean values (± SD) and the individual outer hair cell (OHC) counts are shown by the open symbols. Numbers above the data represent the number of mice and OHCs used for each time point.

region of 140 μm of the apical coil (9–12 kHz), was not significantly reduced between 1 and 6 months (C3H: $P = 0.4595$; 6N: $P = 0.5089$; 6N-Repaired: $P = 0.2419$, Tukey's post hoc test, two-way ANOVA). However, between 1 and 15 months, the number of SK2 puncta was significantly reduced in 6N, 6N-Repaired and 6J ($P = 0.0005$, $P = 0.0030$, $P < 0.0001$, respectively, Tukey's post hoc test, one-way ANOVA) but not in C3H mice ($P = 0.6580$) (Fig. 9C). We also found that the percentage of most of the SK2 channels in OHCs were juxtaposed with ChAT staining (Fig. 9D), with no significant age-related changes in all mouse strains ($P = 0.7668$, two-way ANOVA). However, some OHCs showed only efferent terminals (Fig. 9A,B, arrowheads) or SK2 channels (Fig. 9A,B, arrows).

Mechanoelectrical transduction is reduced in OHCs from ageing mice

Another key biophysical property of hair cells is their ability to convert sound into an electrical signal, a process performed by the MET apparatus. The gross morphology

of the OHC stereociliary bundles appeared normal in the apical coil of aged 6N mice (Fig. 10A; see also Bullen *et al.* 2019), despite their elevated ABR and DPOAE thresholds (Figs 1–3). We therefore investigated whether other properties of the MET apparatus had changed in ageing mice. Quantitative PCR revealed that the expression of *Cdh23* was significantly reduced at 15 months of age in both 6N and 6J mice ($P = 0.0119$ and $P < 0.0001$, respectively, Student's *t* test, Fig. 10B). A reduction in *Cdh23* expression also occurred in the 6N-Repaired strain ($P = 0.0073$), which have overall better hearing than both 6N and 6J mice, and like CBA (Sha *et al.* 2008; Sergeyenko *et al.* 2013) are unlikely to lose many OHCs along the cochlea at old ages. On the other hand, *Pcdh15* (protocadherin-15) was significantly increased in 6N and 6J ($P = 0.0375$ and $P = 0.0057$, respectively) but not in 6N-Repaired mice ($P = 0.0891$, Student's *t* test, Fig. 10B). These data indicate that despite the normal morphology of the stereociliary bundles, the function of the MET apparatus is likely to change in the ageing cochlea, which could be investigated by recording the MET current. However, recording the MET current in OHCs is usually

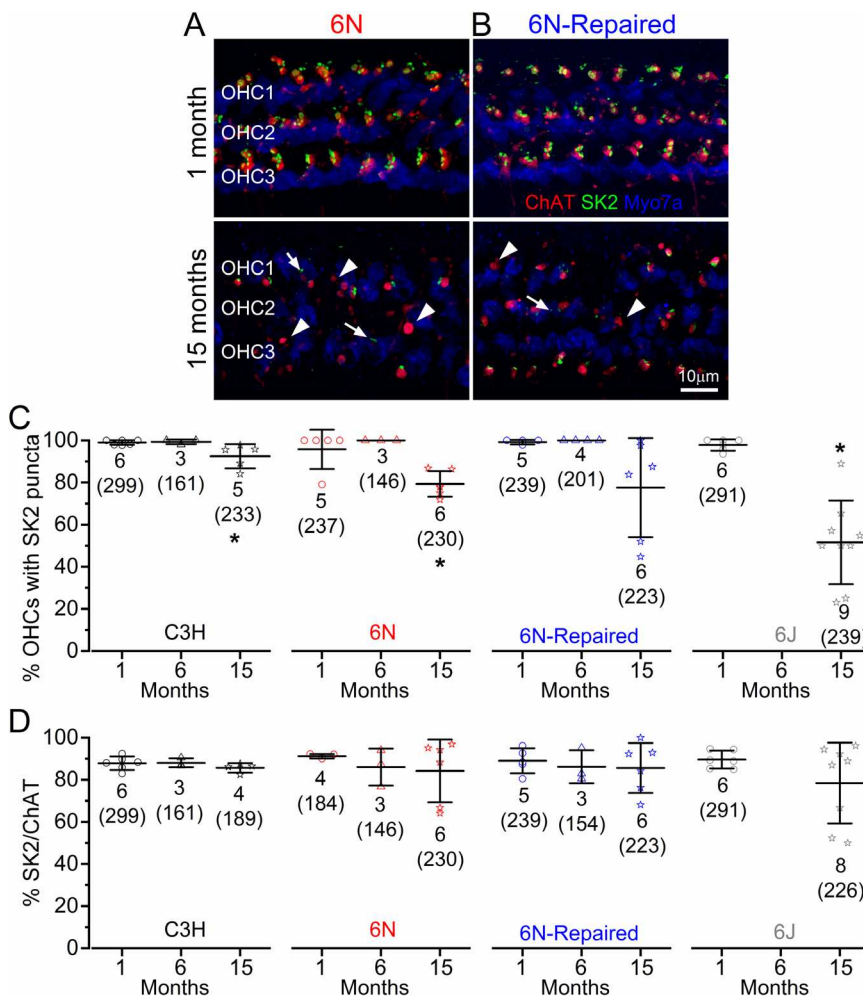


Figure 9. Efferent synapses are present in aged outer hair cells

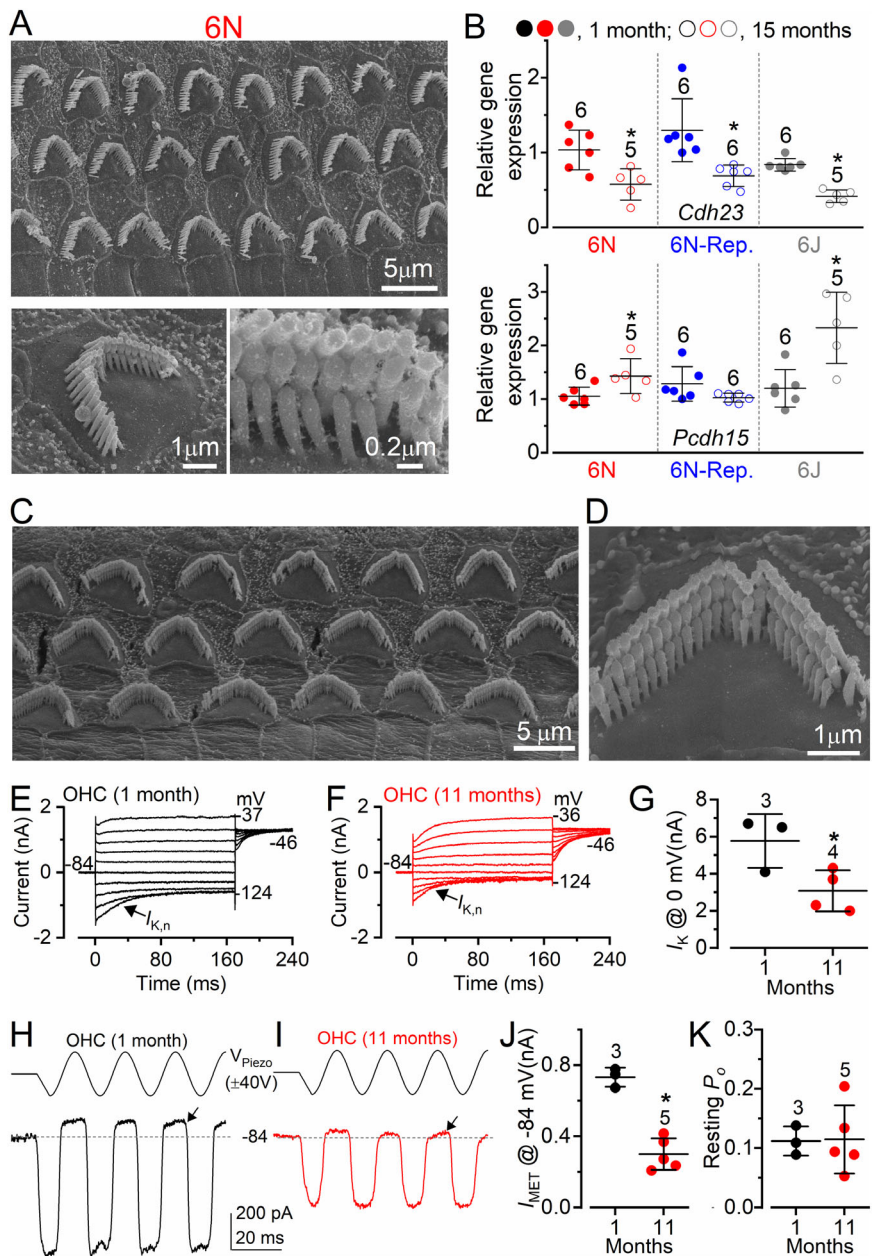
A and B, maximum intensity projections of confocal z-stacks taken from the apical cochlear region of 6N (A) and 6N-Repaired (B) mice at 1 and 15 months of age using antibodies against SK2 (green) and ChAT (red). Myosin 7a (Myo7a) was used as a hair cell marker. Arrowheads indicate outer hair cells with only efferent terminals; and arrows indicate OHCs with only anti-SK2 signals. Scale bars: 10 μm . C, number of SK2 puncta per OHCs present in a 140 μm apical cochlea region as a function of age in C3H, 6N, 6N-Repaired and 6J mice. D, percentage of juxtaposed SK2 and ChAT puncta as a function of age and strain. Data are plotted as mean values (\pm SD) and individual OHC counts are indicated by the open symbols. Numbers below the data in panel C represent the number of mice and (OHCs) used for each time point, which also apply to panel D.

limited to pre-hearing ages because of the difficulties associated with making measurements from adult hair cells. Furthermore, the stereociliary bundles of OHCs are easily damaged during the physical removal of the attached TM. In order to provide some information on possible changes in the MET current with age, we attempted a few recordings from mice (*Tecta/b^{-/-}*: see Methods), in which the TM is not attached to the OHC stereociliary bundles and as such its removal does not disrupt the classical V-shaped bundle structure (Fig. 10C, D). As for the 6J and 6N strains, we found that these *Tecta/b^{-/-}* mice, which are primarily on the 6N background, harbour the *Cdh23^{ahl}* allele. The OHCs of 11-month-old *Tecta/b^{-/-}*

mice were all present in the 9–12 kHz cochlear region, and their basolateral current profile was comparable to that of 1-month-old OHCs (Fig. 10E, F), but with a significantly reduced K⁺ current ($P = 0.0373$, Student's *t* test, Fig. 10G), as also shown for the other mouse strains (Fig. 5C). Using these *Tecta/b^{-/-}* mice, we showed that a large MET current was present in OHCs from both 1-month and 11-month-old mice (Fig. 10H–I), although in aged cells it was significantly reduced compared with 1 month ($P = 0.0003$, Student's *t* test, Fig. 10J). Despite the different MET current size, the open probability of MET channels at rest and in 1.3 mM Ca²⁺ was comparable between the two ages ($P = 0.9403$, Fig. 10K). These data

Figure 10. Changes in the mechanoelectrical transducer apparatus in ageing outer hair cells

A, scanning electron microscopy (SEM) showing the gross morphology of the outer hair cell (OHC) stereociliary bundle from 1-year-old 6N mice in the 8 kHz cochlear region. B, quantitative real-time PCR (qPCR) from organ of Corti RNA, from 6N, 6J and 6N-Repaired mice at 1 and 15 months of age. Genes investigated: *Cdh23* (cadherin 23) and *Pcdh15* (protocadherin 15). Number of mice tested is shown above the columns. Data are shown as means ± SD. C and D, SEM showing the gross morphology of the OHC stereociliary bundle from aged *Tecta/b^{-/-}* mice. E and F, examples of K⁺ currents recorded from apical-coil OHCs of 1 month (E) and 11 month (F) *Tecta/b^{-/-}* mice. Currents were recorded using the voltage protocol described in Fig. 4. G, peak K⁺ current (I_K) measured from *Tecta/b^{-/-}* mouse OHCs at the step potential of 0 mV, from the holding of -84 mV, at 1 and 11 months of age. H and I, saturating MET currents recorded from OHCs of 1 month (H) and 11 month (I) *Tecta/b^{-/-}* mice by applying sinusoidal force stimuli of 50 Hz to the hair bundles from a holding potential of -84 mV. The driver voltage (V_{Piezo}) signal of ± 40 V to the fluid jet is shown above the traces (positive half-cycles of the V_{Piezo} are inhibitory). The extracellular Ca²⁺ concentration was 1.3 mM. The arrows indicate the complete closure of the transducer currents elicited during inhibitory bundle displacements (note that the difference in current between this level and the dashed lines represents the size of the resting MET current). Dashed lines indicate the holding current, which is the current at the holding membrane potential. J and K, maximal size (J) and resting open probability (K) of the MET current recorded at the two different ages from OHCs of *Tecta/b^{-/-}* mice. The number of OHCs tested is shown above the data points.



suggest the intriguing possibility that changes in the MET current with age could be a mechanism involved in the progression of ARHL in ageing mice, at least in those harbouring the *Cdh23^{ahl}* allele as previously suggested (Johnson *et al.* 1997; Noben-Trauth *et al.* 2003; Johnson *et al.* 2017).

Discussion

In this study, we have provided evidence that several of the biophysical properties of OHCs remained unaffected by ageing. Despite the highly elevated DPOAE thresholds in the ~12 kHz cochlear region of aged early-onset hearing loss (6N and 6J) compared with C3H and 6N-Repaired mice, OHCs exhibited similar basolateral membrane characteristics irrespective of mouse strain. The first morphological alteration we observed in ageing OHCs (9–12 kHz region) was the reduction in their surface area, which was already evident in 6N, 6J and C3H mice at 6 months of age. The reduction in OHC surface area was not a sign of apoptosis in this case, since OHC loss was minimal even in 14–16-month-old mice, and did not significantly affect DPOAEs in C3H and C57BL/6NTac^{*Cdh23*⁺} mice. In addition, OHCs showed a reduction in the basolateral K⁺ current size and electromotile activity, which was proportional to their smaller membrane surface area, but remained viable with normal resting membrane potentials. The size, but not the open probability of the MET current was also reduced in aged OHCs compared with young adult cells. At the synaptic level, the loss of afferent and efferent synapses was evident at 15 months. OHCs from C3H mice, which showed the best hearing profile at 12 kHz, exhibited very little change to their efferent synapse architecture in old mice, highlighting specific genetic background differences. We propose that with ageing, the basolateral membrane of OHCs undergoes several biophysical and morphological changes (Fig. 11). We have also provided evidence that the MET current of OHCs from mice harbouring the *Cdh23^{ahl}* allele is reduced with age, highlighting the possibility that it could be playing a crucial role in ARHL.

Age-related hearing loss in different mouse strains

The mouse has become the primary animal model to study ageing in the auditory system (Ohlemiller *et al.* 2016; Bowl & Dawson, 2019). The commonly used 6J (C57BL/6J) and 6N (C57BL/6NTac) mice have a single-nucleotide polymorphism in exon7 of the *cadherin23* (*Cdh23^{ahl}* or *Cdh23^{753A}*; Johnson *et al.* 1997; Noben-Trauth *et al.* 2003; Johnson *et al.* 2017), which causes them to already exhibit hearing loss in the high-frequency region by 3–6 months and become almost completely deaf by 15 months of age

(Hequembourg & Liberman, 2001; Kane *et al.* 2012). The *Cdh23^{ahl}* allele is present in several of the early-onset, but not in the late-onset hearing loss mouse strains, such as C3H mice (Trune *et al.* 1996). To investigate the possible involvement of strain-specific effects, we have also used the 6N co-isogenic C57BL/6NTac^{*Cdh23*⁺} mice (6N-Repaired), in which the *Cdh23^{ahl}* allele was repaired with targeted CRISPR/Cas9 gene editing (Mianné *et al.* 2016). We found that, compared with the C3H and 6N-Repaired strains, aged mice from both ‘early-onset hearing loss’ strains (6N and 6J) had significantly raised ABR and DPOAE thresholds as previously shown (e.g. Parham, 1997; Spongr *et al.* 1997; Jimenez *et al.* 1999; Zheng *et al.* 1999; Hequembourg & Liberman, 2001; Sha *et al.* 2008). Although sex differences in DPOAE thresholds have been described in CBA mice, they normally occur starting from 14–16 months (Guimaraes *et al.* 2004), which is just after the age at which we performed the recordings in the four mouse strains. In the frequency region used to investigate the morphological and physiological properties of OHCs (9–12 kHz), DPOAE thresholds were similar in all four mouse strains until about 9 months of age, but became significantly raised thereafter in both 6N and 6J mice.

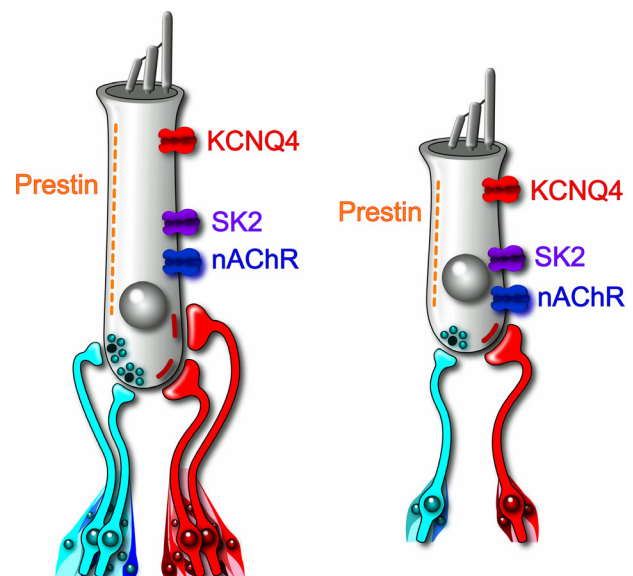


Figure 11. Schematic representation of the biophysical and morphological profile of young adult and aged outer hair cells

A and B, schematic representation of the basolateral membrane protein profile and innervation pattern of outer hair cells (OHCs) from young adult and aged 6N, 6J, C3H and 6N-Repaired mice. Note the reduction in size of OHCs that leads to the reduction in numbers of all the indicated membrane proteins in OHCs. The afferent (blue) and efferent (red) fibres are present at both ages, but become reduced in number in aged OHCs.

The reduced surface area of OHCs is an early sign of cochlear ageing

We have shown that the surface area of aged OHCs is smaller than that measured in young adult OHCs. Although cellular shrinkage is generally associated with apoptotic mechanisms, this is not the case for the OHCs. At a time when the reduction in surface area was already present in all OHCs from 6-month-old mice (9–12 kHz cochlea region), we found no OHC loss in any of the four mouse strains. Moreover, in 14–16-month-old mice only about 20% of the apical OHCs were missing, which is consistent with previous reports for both C57BL/6 (Hequembourg & Liberman, 2001; Francis *et al.* 2003; Zachary & Fuchs, 2015) and CBA mice (Sha *et al.* 2008; Ohlemiller *et al.* 2010; Sergeyenko *et al.* 2013). The normal DPOAE thresholds in aged C3H and 6N-Repaired mice, despite having fewer OHCs present in the apical coil, are likely to be due to the smaller contribution of cochlear amplification for low-frequency sounds compared with higher-frequency sounds (Liberman *et al.* 2002).

The presence of healthy OHCs despite a reduced surface area is also supported by a previous study showing that cell shrinkage is a morphological change that can be separate from apoptosis (Bortner & Cidlowski, 2003). There are several lines of evidence indicating that a cell's size can be adaptively regulated to an optimal volume in response to a variety of physiological stimuli (Ginzberg *et al.* 2015; Miettinen & Björklund, 2016), with larger cells tending to have higher metabolic activities (Giordano *et al.* 1993; Ginzberg *et al.* 2015; Miettinen & Björklund, 2016). The cochlea has been shown to be highly dependent on energy provided by mitochondria, and their dysfunction exacerbates the progression of ARHL (Pickles, 2004; Crawley & Keithley, 2011). Therefore, it is possible that the reduction in OHC size reduces energy consumption, thus maintaining functionality. Since a similar temporal progression in the reduction in size and loss of OHCs is present in both 'early-onset hearing loss' (6J and 6N) and C3H and 6N-Repaired mice, they are unlikely to contribute directly to their different DPOAE thresholds, implicating OHC reduction in size as a general trait in the normal pathophysiological changes in the cochlea with age.

Changes in the physiology of OHCs with age

In addition to the reduction in OHC surface area, we observed a decrease in the size of basolateral K^+ current $I_{K,n}$ and non-linear capacitance (NLC). However, when the size of $I_{K,n}$ and NLC were normalized to OHC surface area they were comparable with those in younger cells, suggesting that the loss of OHC membrane is responsible for the loss of proteins. A reduced OHC surface area and loss of prestin has also recently been shown in OHCs

from 8 month old C57BL/6 mice (Bai *et al.* 2019). In addition to the loss of basolateral membrane channels and prestin, aged OHCs showed a similar progressive loss of afferent synapses irrespective of the mouse strain. This seemed to also correlate with the reduction in OHC surface area since their number was still normal at 6 months of age. The efferent synapses were also largely affected with age. However, these age-related changes were minimal or absent in C3H mice, which have the better hearing profile. Despite the progressive reduction in basolateral membrane currents, the *in vitro* resting membrane potential (V_m) remained similar between young and aged OHCs and to that previously reported (Marcotti & Kros, 1999). The consistency in resting V_m with age indicates that OHCs are likely to be viable and functional, which is also suggested by the normal DPOAE thresholds in aged C3H and 6N-Repaired mice. Therefore, similar to the reduction in OHC size, the above biophysical and synaptic changes appear to be a general mechanism that maintains cell function in the ageing cochlea. One change that seems to be independent from the smaller basolateral membrane surface area was the reduction of the MET current. These data provide the intriguing hypothesis that the early-onset hearing loss in mice harbouring the *Cdh23^{ahl}* allele could be due to defects in the MET apparatus. Being able to directly address this hypothesis will require the generation of the *Tecta/b^{-/-}* mouse on the 6N-Repaired background. However, we recently found that in IHCs, whose stereocilia are not attached to the TM and, therefore, less damaged by its removal, the MET current was found significantly smaller in mice harbouring the hypomorphic *Cdh23* allele *Cdh23^{ahl}* compared with that measured in IHCs from 6N-Repaired mice (data not shown).

Mechanisms leading to progressive hearing loss with age

Our results have shown that in the apical coil (9–12 kHz) of the aged cochlea from all four mouse strains, OHCs retained similar resting membrane potentials to those measured in cells from young adult mice. Although the basolateral membrane protein profile of OHCs from all mouse strains was retained at older ages, the expression level of different proteins was significantly reduced compared with that found in young adult cells, most likely due to their reduced surface area (Fig. 11). The extent of OHC and afferent loss with age was comparable between all four mouse strains, indicating that these age-related changes are a general characteristic of the ageing cochlea. The loss of efferent synapses appeared strain-specific because it was very minimal or absent in C3H mice, which is the best-hearing strain.

Our finding that MET current size is reduced in ageing mice carrying the *Cdh23^{ahl}* allele is consistent with previous work showing that this allele is likely to be

responsible for the early-onset hearing loss phenotype in 6J and 6N mice (Johnson *et al.* 1997; Noben-Trauth *et al.* 2003), which agrees with our finding of a reduction in MET current size with ageing in mice with the *Cdh23^{ahl}* allele. The contribution of the MET apparatus to ARHL is also supported by the progressive alteration in the structural and functional integrity of the stereociliary bundles observed with age in the chinchilla, mouse and human (Bohne *et al.* 1990; Bullen *et al.* 2019). Additional functional alterations in hair cells that could contribute to the progression of hearing loss with age include the biophysical properties of IHCs and their synapses, with the latter also being correlated with the degree of hearing loss in mice (data not shown).

References

- Abe T, Kakehata S, Kitani R, Maruya S, Navaratnam D, Santos-Sacchi J & Shinkawa H (2007). Developmental expression of the outer hair cell motor prestin in the mouse. *J Membr Biol* **215**, 49–56.
- Ashmore J (2008). Cochlear outer hair cell motility. *Physiol Rev* **88**, 173–210.
- Ashmore J (2019). Outer hair cells and electromotility. *Cold Spring Harb Perspect Med* pii, a033522.
- Ashmore JF (1987). A fast motile response in guinea-pig outer hair cells: the cellular basis of the cochlear amplifier. *J Physiol* **388**, 323–347.
- Bai JP, Navaratnam D & Santos-Sacchi J (2019). Prestin kinetics and corresponding frequency dependence augment during early development of the outer hair cell within the mouse organ of Corti. *Sci Rep* **9**, 16460.
- Belyantseva IA, Adler HJ, Curi R, Frolenkov GI & Kachar B (2000). Expression and localization of prestin and the sugar transporter GLUT-5 during development of electromotility in cochlear outer hair cells. *J Neurosci* **20**, RC116.
- Bohne BA, Gruner MM & Harding GW (1990). Morphological correlates of aging in the chinchilla cochlea. *Hear Res* **48**, 79–91.
- Bortner CD & Cidlowski JA (2003). Uncoupling cell shrinkage from apoptosis reveals that Na⁺ influx is required for volume loss during programmed cell death. *J Biol Chem* **278**, 39176–39184.
- Bowl MR & Dawson SJ (2019). Age-related hearing loss. *Cold Spring Harb Perspect Med* **9**, a033217.
- Bowl MR, Simon MM, Ingham NJ, Greenaway S, Santos L, Cater H, Taylor S, Mason J, Kurbatova N, Pearson S, Bower LR, Clary DA, Meziiane H, Reilly P, Minowa O, Kelsey L; International Mouse Phenotyping Consortium, Tocchini-Valentini GP, Gao X, Bradley A, Skarnes WC, Moore M, Beaudet AL, Justice MJ, Seavitt J, Dickinson ME, Wurst W, de Angelis MH, Herault Y, Wakana S, Nutter LMJ, Flenniken AM, McKerlie C, Murray SA, Svenson KL, Braun RE, West DB, Lloyd KCK, Adams DJ, White J, Karp N, Flicek P, Smedley D, Meehan TF, Parkinson HE, Teboul LM, Wells S, Steel KP, Mallon AM & Brown SDM (2017). A large scale hearing loss screen reveals an extensive unexplored genetic landscape for auditory dysfunction. *Nat Comm* **8**, 886.
- Brownell WE, Bader CR, Bertrand D & de Ribaupierre Y (1985). Evoked mechanical responses of isolated cochlear outer hair cells. *Science* **227**, 194–196.
- Bullen A, Forge A, Wright A, Richardson GP, Goodyear RJ & Taylor R (2019). Ultrastructural defects in stereocilia and tectorial membrane in aging mouse and human cochleae. *J Neurosci Res* <https://doi.org/10.1002/jnr.24556>.
- Ceriani F, Hendry A, Jeng JY, Johnson SL, Stephani F, Olt J, Holley MC, Mammano F, Engel J, Kros CJ, Simmons DD & Marcotti W (2019). Coordinated calcium signalling in cochlear sensory and non-sensory cells refines afferent innervation of outer hair cells. *EMBO J* **38**, pii: e99839.
- Corns LF, Johnson SL, Kros CJ & Marcotti W (2014). Calcium entry into stereocilia drives adaptation of the mechano-electrical transducer current of mammalian cochlear hair cells. *Proc Natl Acad Sci USA* **111**, 14918–14923.
- Corns LF, Johnson SL, Roberts T, Ranatunga KM, Hendry A, Ceriani F, Safieddine S, Steel KP, Forge A, Petit C, Furness DN, Kros CJ & Marcotti W (2018). Mechanotransduction is required for establishing and maintaining mature inner hair cells and regulating efferent innervation. *Nature Comm* **9**, 4015.
- Crawley BK & Keithley EM (2011). Effects of mitochondrial mutations on hearing and cochlear pathology with age. *Hear Res* **280**, 201–208.
- Francis HW, Ryugo DK, Gorelikow MJ, Prosen CA & May BJ (2003). The functional age of hearing loss in a mouse model of presbycusis. II. Neuroanatomical correlates. *Hear Res* **183**, 29–36.
- Fuchs PA (2003). The diversified form and function of cochlear afferents. In: *The Oxford Handbook of the Auditory Brainstem*, ed. Kandler K, pp. 1–26. Oxford University Press. <https://doi.org/10.1093/oxfordhb/9780190849061.013.2>
- Fuchs PA & Lauer AM (2019). Efferent Inhibition of the Cochlea. *Cold Spring Harb Perspect Med* **9**, pii: a033530.
- Furness DN & Hackney CM (1986). High-resolution scanning-electron microscopy of stereocilia using the osmium-thiocarbonylhydrazide coating technique. *Hear Res* **21**:243–249.
- Gates GA & Mills JH (2005) Presbycusis. *Lancet* **366**, 1111–1120.
- Ginzberg MB, Kafri R & Kirschner M (2015). Cell biology. On being the right (cell) size. *Science* **348**, 1245075.
- Giordano E, Cirulli V, Bosco D, Rouiller D, Halban P & Meda P (1993). B-cell size influences glucose-stimulated insulin secretion. *Am J Physiol-Cell Physiol* **265**, C358–C364
- Goodyear RJ, Cheatham MA, Naskar S, Zhou Y, Osgood RT, Zheng J & Richardson GP (2019). Accelerated age-related degradation of the tectorial membrane in the *Ceacam16^{βgal/βgal}* null mutant mouse, a model for late-onset human hereditary deafness DFNB113. *Front Mol Neurosci* **12**, 147.
- Gordon-Salant S (2005). Hearing loss and aging: new research findings and clinical implications. *J Rehabil Res Dev* **42**, 9–24.
- Guimaraes P, Zhu X, Cannon T, Kim S & Frisina RD (2004). Sex differences in distortion product otoacoustic emissions as a function of age in CBA mice. *Hear Res* **192**, 83–89.
- Guinan JJ, Jr (1996). Physiology of olivocochlear efferents. In *The Cochlea*, ed. Dallos P, Popper AN & Fay RR, pp. 435–502. Springer, New York.

- Hequembourg S & Liberman MC (2001). Spiral ligament pathology: a major aspect of age-related cochlear degeneration in C57BL/6 mice. *J Assoc Res Otolaryngol* **2**, 118–129.
- Huang G & Santos-Sacchi J (1993). Mapping the distribution of the outer hair cell motility voltage sensor by electrical amputation. *Biophys J* **65**, 2228–2236.
- Ingham NJ, Pearson S & Steel KP (2011). Using the auditory brainstem response (abr) to determine sensitivity of hearing in mutant mice. *Curr Protoc Mouse Biol* **1**, 279–287.
- Jeng JY, Ceriani F, Hendry A, Johnson SL, Yen P, Simmons DD, Kros CJ & Marcotti W (2020). Hair cell maturation is differentially regulated along the tonotopic axis of the mammalian cochlea. *J Physiol* **598**, 151–170.
- Jimenez AM, Stagner BB, Martin GK & Lonsbury-Martin BL (1999). Age-related loss of distortion product otoacoustic emissions in four mouse strains. *Hear Res* **38**, 91–105.
- Johnson KR, Erway LC, Cook SA, Willott JF & Zheng QY (1997). A major gene affecting age-related hearing loss in C57BL/6J mice. *Hear Res* **114**, 83–92.
- Johnson KR, Tian C, Gagnon LH, Jiang H, Ding D & Salvi R (2017). Effects of *Cdh23* single nucleotide substitutions on age-related hearing loss in C57BL/6 and 129S1/Sv mice and comparisons with congenic strains. *Scientific Reports* **7**, 44450.
- Johnson SL, Beurg M, Marcotti W & Fettiplace R (2011). Prestin-driven cochlear amplification is not limited by the outer hair cell membrane time constant. *Neuron* **70**, 1143–1154.
- Kane KL, Longo-Guess CM, Gagnon LH, Ding D, Salvi RJ & Johnson KR (2012). Genetic background effects on age-related hearing loss associated with *Cdh23* variants in mice. *Hear Res* **283**, 80–88.
- Katz E, Elgoyhen AB, Gomez-Casati ME, Knipper M, Vetter DE, Fuchs PA & Glowatzki E (2004). Developmental regulation of nicotinic synapses on cochlear inner hair cells. *J Neurosci* **24**, 7814–7820.
- Kazmierczak P, Sakaguchi H, Tokita J, Wilson-Kubalek EM, Milligan RA, Muller U & Kachar B (2007). Cadherin 23 and protocadherin 15 interact to form tip-link filaments in sensory hair cells. *Nature* **449**, 87–91.
- Kenyon EJ, Kirkwood NK, Kitcher SR, O'Reilly M, Derudas M, Cantillon DM, Goodyear RJ, Secker A, Baxendale S, Bull JC, Waddell SJ, Whitfield TT, Ward SE, Kros CJ & Richardson GP (2017). Identification of ion-channel modulators that protect against aminoglycoside-induced hair cell death. *JCI Insight* **2**, e96773.
- Kubisch C, Schroeder BC, Friedrich T, Lütjohann B, El-Amraoui A, Marlin S, Petit C & Jentsch TJ (1999). KCNQ4, a novel potassium channel expressed in sensory outer hair cells, is mutated in dominant deafness. *Cell* **96**, 437–446.
- Kusunoki T, Cureoglu S, Schachern PA, Baba K, Kariya S & Paparella MM (2004). Age-related histopathologic changes in the human cochlea: a temporal bone study. *Otolaryngol Head Neck Surg* **131**, 897–903.
- Liberman MC (1980). Efferent synapses in the inner hair cell area of the cat cochlea: an electron microscopic study of serial sections. *Hear Res* **3**, 189–204.
- Liberman MC (2017). Noise-induced and age-related hearing loss: new perspectives and potential therapies. *F1000Res* **6**, 927
- Liberman MC, Gao J, He DZ, Wu X, Jia S & Zuo J (2002). Prestin is required for electromotility of the outer hair cell and for the cochlear amplifier. *Nature* **419**, 300–304.
- Lioudyno M, Hiel H, Kong JH, Katz E, Waldman E, Parameshwaran-Iyer S, Glowatzki E & Fuchs PA (2004). A “synaptoplasmic cistern” mediates rapid inhibition of cochlear hair cells. *J Neurosci* **24**, 11160–11164.
- Mahendrasingam S, Beurg M, Fettiplace R & Hackney CM (2010). The ultrastructural distribution of prestin in outer hair cells: a post-embedding immunogold investigation of low-frequency and high-frequency regions of the rat cochlea. *Eur J Neurosci* **31**, 1595–1605.
- Maison SF, Adams JC & Liberman MC (2003). Olivocochlear innervation in the mouse: immunocytochemical maps, crossed versus uncrossed contributions and transmitter colocalization. *J Comp Neurol* **455**, 406–416.
- Mammano F & Ashmore J (1996). Differential expression of outer hair cell potassium currents in the isolated cochlea of the guinea-pig. *J Physiol* **496**, 639–646.
- Marcotti W, Johnson SL & Kros CJ (2004). A transiently expressed SK current sustains and modulates action potential activity in immature mouse inner hair cells. *J Physiol* **560**, 691–708
- Marcotti W & Kros CJ (1999). Developmental expression of the potassium current $I_{K,n}$ contributes to maturation of mouse outer hair cells. *J Physiol* **520**, 653–660.
- Mianné J, Chessum L, Kumar S, Aguilar C, Codner G, Hutchison M, Parker A, Mallon AM, Wells S, Simon MM, Teboul L, Brown SD & Bowl MR (2016). Correction of the auditory phenotype in C57BL/6N mice via CRISPR/Cas9-mediated homology directed repair. *Genome Med* **8**, 16.
- Miettinen TP & Björklund M (2016). Cellular allometry of mitochondrial functionality establishes the optimal cell size. *Dev Cell* **39**, 370–382
- Müller M, von Hünerbein K, Hoidis S & Smolders JW (2005). A physiological place-frequency map of the cochlea in the CBA/J mouse. *Hear Res* **202**, 63–73.
- Noben-Trauth K, Zheng QY & Johnson KR (2003). Association of cadherin 23 with polygenic inheritance and genetic modification of sensorineural hearing loss. *Nat Genet* **35**, 21–23.
- Ohlemiller KK (2006). Contributions of mouse models to understanding of age- and noise-related hearing loss. *Brain Res* **1091**, 89–102.
- Ohlemiller KK, Dahl AR & Gagnon PM (2010). Divergent aging characteristics in CBA/J and CBA/CAJ mouse cochleae. *J Assoc Res Otolaryngol* **11**, 605–623.
- Ohlemiller KK, Jones SM & Johnson KR (2016). Application of mouse models to research in hearing and balance. *J Assoc Res Otolaryngol* **17**, 493–523.
- Oliver D & Fakler B (1999). Expression density and functional characteristics of the outer hair cell motor protein are regulated during postnatal development in rat. *J Physiol* **51**, 791–800.

- Oliver D, Klöcker N, Schuck J, Baukowitz T, Ruppertsberg JP & Fakler B (2000). Gating of Ca²⁺-activated K⁺ channels controls fast inhibitory synaptic transmission at auditory outer hair cells. *Neuron* **26**, 595–601.
- Oliver D, He DZ, Klöcker N, Ludwig J, Schulte U, Waldegger S, Ruppertsberg JP, Dallos P & Fakler B (2001). Intracellular anions as the voltage sensor of prestin, the outer hair cell motor protein. *Science* **292**, 2340–2343.
- Parham K (1997). Distortion product otoacoustic emissions in the C57BL/6J mouse model of age-related hearing loss. *Hear Res* **112**, 216–234.
- Pickles JO (2004). Mutation in mitochondrial DNA as a cause of presbycusis. *Audiol Neurootol* **9**, 23–33.
- Richardson GP, de Monvel JB & Petit C (2011). How the genetics of deafness illuminates auditory physiology. *Annu Rev Physiol* **73**, 311–334.
- Ryugo DK (1992). The auditory nerve: peripheral innervation, cell body morphology, and central projections. In *The Mammalian Auditory Pathway: Neuroanatomy*, ed. Webster DB, Popper AN, Fay RR, pp. 23–65. Springer, New York.
- Sergeyenko Y, Lall K, Liberman MC & Kujawa SG (2013). Age-related cochlear synaptopathy: an early-onset contributor to auditory functional decline. *J Neurosci* **33**, 13686–13694.
- Sha SH, Kanicki A, Dootz G, Talaska AE, Halsey K, Dolan D, Altschuler R & Schacht J (2008). Age-related auditory pathology in the CBA/J mouse. *Hear Res* **243**, 87–94.
- Simmons DD, Mansdorf NB & Kim JH (1996). Olivocochlear innervation of inner and outer hair cells during postnatal maturation: evidence for a waiting period. *J Comp Neurol* **370**, 551–562.
- Simmons DD, Tong B, Schrader AD & Hornak AJ (2010). Oncomodulin identifies different hair cell types in the mammalian inner ear. *J Comp Neurol* **518**, 3785–3802.
- Spongr VP, Flood DG, Frisina RD & Salvi RJ (1997). Quantitative measures of hair cell loss in CBA and C57BL/6 mice throughout their life spans. *J Acoust Soc Am* **101**, 3546–3553.
- Trune DR, Kempton JB & Mitchell C (1996). Auditory function in the C3H/HeJ and C3H/HeSnJ mouse strains. *Hear Res* **96**, 41–45.
- Zachary SP & Fuchs PA (2015). Re-emergent inhibition of cochlear inner hair cells in a mouse model of hearing loss. *J Neurosci* **35**, 9701–9706.
- Zheng J, Shen W, He DZ, Long KB, Madison LD & Dallos P (2000). Prestin is the motor protein of cochlear outer hair cells. *Nature* **405**, 149–155.
- Zhai F, Song L, Bai JP, Dai C, Navaratnam D & Santos-Sacchi J (2020). Maturation of voltage-induced shifts in SLC26a5 (prestin) operating point during trafficking and membrane insertion. *Neurosci* **431**, 128–133.
- Zheng QY, Johnson KR & Erway LC (1999). Assessment of hearing in 80 inbred strains of mice by ABR threshold analyses. *Hear Res* **130**, 94–107.

Additional information

Data availability statement

The data that support the findings of this study are available from the corresponding author upon reasonable request.

Competing interests

The Authors declare no conflicts of interest.

Author contributions

J-YJ, SLJ, AJC, LDeT, RG, DNE, GPR, MCH, MM and WM were involved in the acquisition, analysis or interpretation of data for the work. SW, SDB, MRB were involved in the initial design and interpretation of data. J-YJ, SLJ, AJC, LDeT, RG, DNE, SW, SDB, GPR, MCH, MM, MRB and WM were involved in revising it critically for important intellectual content. J-YJ and WM conceived and designed the study and drafted the paper.

All authors approved the final version of the manuscript. All authors agree to be accountable for all aspects of the work in ensuring that questions related to the accuracy or integrity of any part of the work are appropriately investigated and resolved. All persons designated as authors qualify for authorship, and all those who qualify for authorship are listed.

Funding

This work was supported by: the Wellcome Trust (102892/Z/13/Z) to WM; the Medical Research Council (MC/UP/1503/2) to MRB and (MR/S002510/1) to MM. AJC is funded by a PhD studentship from Action on Hearing Loss (S50).

Acknowledgements

The authors thank Lukas Rüttiger for advice on the DPOAE analysis, Neil Ingham for advice on ABR measurements, and Michelle Bird for her assistance with the mouse colonies.

Keywords

ageing, cochlea, electromotility, hearing loss, ion channels, mechano-electrical transduction, mouse, OHCs

Supporting information

Additional supporting information may be found online in the Supporting Information section at the end of the article.

Statistical Summary Document